Neurosurg Clin N Am 14 (2003) 55–80

NEUROSURGERY CLINICS OF NORTH AMERICA

Imaging of the pituitary and parasellar region

Chi S. Zee, MD*, John L. Go, MD, Paul E. Kim, MD, David Mitchell, MD, Jamshid Ahmadi, MD

Department of Imaging, University of Southern California University Hospital, 1500 San Pablo Street, Los Angeles, CA 90033, USA

Normal pituitary anatomy

The pituitary gland sits in the bony pituitary fossa, which is superior to the sphenoid sinus. The pituitary gland is an oblong structure that measures approximately 12 mm transversely, 10 mm anteroposteriorly, and 7 mm in height. The superior margin of the pituitary gland is usually flat except in girls and young women, in whom the pituitary gland may be convex superiorly. A number of studies have been performed to determine the normal range of height of the pituitary gland in adults. The average height of the pituitary gland in adults measures approximately 5.3 ± 1.7 mm and should never exceed 10 mm (Fig. 1) [1,2]. The pituitary is covered with a thin dural fibrous coat, with a hiatus in the diaphragma sellae that usually measures approximately 5 mm [3]. The pituitary stalk passes through the hiatus in the diaphragma sellae and is connected to the anterior portion of the neurohypophysis (posterior lobe). The adenohypophysis (anterior lobe) constitutes the major portion (three fourths) of the pituitary gland, whereas the neurohypophysis constitutes only one fourth of the gland. The adenohypophysis consists of the pars distalis, pars intermedia, and pars tuberalis, which is an upward extension forming a cuff around the inferior portion of the infundibular stalk. The neurohypophysis consists of the pars nervosa, the infundibular stalk, and the infundibula proper. The pituitary gland has a direct arterial blood supply from the middle and inferior hypophyseal arteries in addition to receiving blood from the portal system. The major blood supply to the adenohypophysis is derived from the hypophyseal portal system, whereas the neurohypophysis is supplied by the middle and inferior hypophyseal arteries of the meningohypophyseal trunk. The pituitary gland is contained within the bony sellar turcica and bordered on either side by the cavernous sinuses. The medial wall of the cavernous sinuses is formed by the thin lateral wall of the pituitary capsule, which is usually not discernable on MRI studies. The lateral wall of the cavernous sinus is a thick dural layer and is well visualized on MRI studies [4]. Densely compacted and heavily granulated cells are seen in the lateral portion of the anterior pituitary lobe, whereas more loosely packed cells are seen centrally in the anterior pituitary lobe [5]. Intercavernous venous connections are present in the diaphragma sellae and in the sellar turcica anterior or inferior to the gland [5,6]. The medial eminence of the tuber cinereum of the hypothalamus is an area rich in peptidergic and catecholaminergic neurons, which secrete into the portal system that drains into the anterior pituitary lobe and regulate its function. The posterior pituitary lobe has no independent secretory function and receives vasopressin and oxytoxin from the hypothalamic neurons through the capillaries. The posterior lobe of the pituitary appears characteristically to exhibit hyperintensity on T1-weighted images on MRI in most patients and seems to lose its hyperintensity gradually with aging [7,8]. In patients with central diabetes insipidus, there is absence of posterior lobe high signal intensity [9]. The high signal intensity

* Corresponding author.
E-mail address: chishing@usc.edu (C.S. Zee).

PII: S1042-3680(02)00034-7

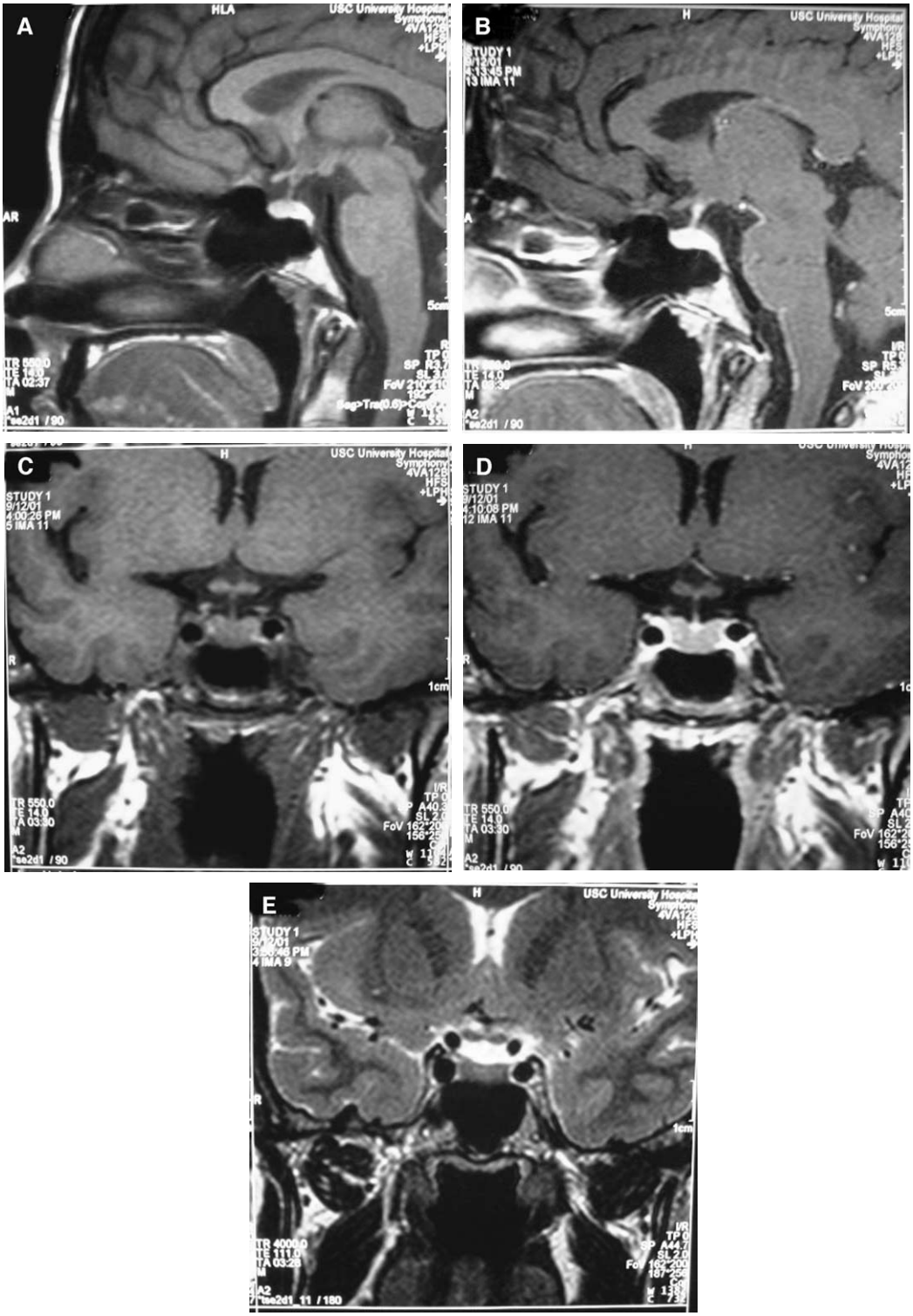
A
B
C
D
E
USC University Hospital

observed in the posterior lobe is thought to represent accumulated secretory product from the hypothalamus.

The anterior pituitary lobe secretes six major hormones. Cells secreting growth hormone constitute most of the cells in the anterior lobe, followed by cells secreting prolactin, thyroid-stimulating hormone, adrenocorticotropic hormone (ACTH), gonadotropin-luteinizing hormone, and follicle-stimulating hormone. Prolactinomas are the most common functioning pituitary tumors, and they tend to be seen in the inferolateral aspect of the anterior lobe.

Normal anatomy of the parasellar region

The pituitary gland lies cupped in a bony outpouching in the skull base known as the sellar turcica, which is within the sphenoid bone. Superiorly, the anterior and posterior clinoid processes demarcate the sellar turcica; inferiorly, the space is defined by the sphenoid sinus anteriorly and the clivus posteriorly. The superior border of the sellar region is the suprasellar cistern. Anteriorly, the space is defined by the convergence of the gyrus recti of the frontal lobes, laterally by the uncus of the temporal lobes, and posteriorly by the cerebral peduncles of the midbrain. The middle cerebral arteries enter the Sylvian fissure at the convergence of the frontal and temporal lobes. The basilar artery lies in the interpeduncular cistern. The optic chiasm and the infundibulum of the pituitary stalk are also in the suprasellar cistern. The cavernous sinuses form the lateral margins of the sellar turcica. The cavernous portion of the internal carotid artery, the abducens nerve, and the cavernous venous space are seen within the cavernous sinus. The oculomotor, trochlear, ophthalmic (V1), and maxillary (V2) branches of the trigeminal nerve lie in the lateral wall of the cavernous sinus. Posteriorly, the mandibular branch (V3) of the trigeminal nerve enters the foramen ovale, and the Gasserian ganglion lies in Meckel's cave.

Imaging techniques

The imaging modality of choice for the pituitary gland is MRI. Coronal CT with contrast and thin slices (1.5–2 mm) may be obtained in patients who have contraindications to MRI. The standard protocol for MRI of the pituitary and parasellar region consists of sagittal T1-weighted images, followed by coronal T1-weighted images performed with and without intravenous contrast. Axial T2-weighted images of the brain are useful to determine the T2 signal intensity of any mass lesion and to have an overview of the brain to exclude other pathologic findings. Coronal T1-weighted images are obtained using thin slices (2.5 mm) and a field of view of less than 200 mm. Axial T2-weighted images of the brain are obtained using 5-mm thick slices. Two hundred fifty-six phase-encoding steps and 256 frequency-encoding steps are used . Contiguous slices with no gap are obtained in the coronal and sagittal planes. For evaluation of pituitary microadenomas, a dynamic contrast-enhanced study is essential to detect subtle lesions. The dynamic study is performed by obtaining five T1-weighted, turbo spin-echo, 3-mm thick slices repetitively 20 seconds, 40 seconds, 60 seconds, 80 seconds, and 100 seconds after the injection of contrast material using an injector. A total of 10 mL of nonionic contrast is injected at the rate of 2 mL/s. The field of view is 190 mm, with 256 frequency-encoding steps and 120 phase-encoding steps. Immediately after the dynamic study, a routine study of the sellar turcica is obtained in coronal and sagittal planes (Fig. 2).

Pituitary adenomas

Pituitary adenomas account for approximately 10% of all intracranial neoplasms. Pituitary adenomas are present in 8% to 27% of routine autopsies of the general population having no evidence of endocrine disease and in children as young as 2 years of age [1,10,11]. These are usually

Fig. 1. Normal pituitary gland. (*A*) Sagittal T1-weighted image shows normal pituitary gland with pituitary stalk. The optic chiasm is seen superior to the stalk. The mamillary body is seen posterior to the chiasm. (*B*) Sagittal postcontrast T1-weighted image shows intense enhancement of the pituitary gland and stalk. (*C*) Coronal T1-weighted image demonstrates a pituitary gland with a flat superior margin. The pituitary stalk is seen in the midline. The optic chiasm is seen superior to the pituitary stalk. The internal carotid artery appears as signal void areas within the cavernous sinus. (*D*) Coronal postcontrast T1-weighted image reveals intense enhancement of the pituitary. (*E*) Coronal T2-weighted image demonstrates the pituitary to be isointense to gray matter.

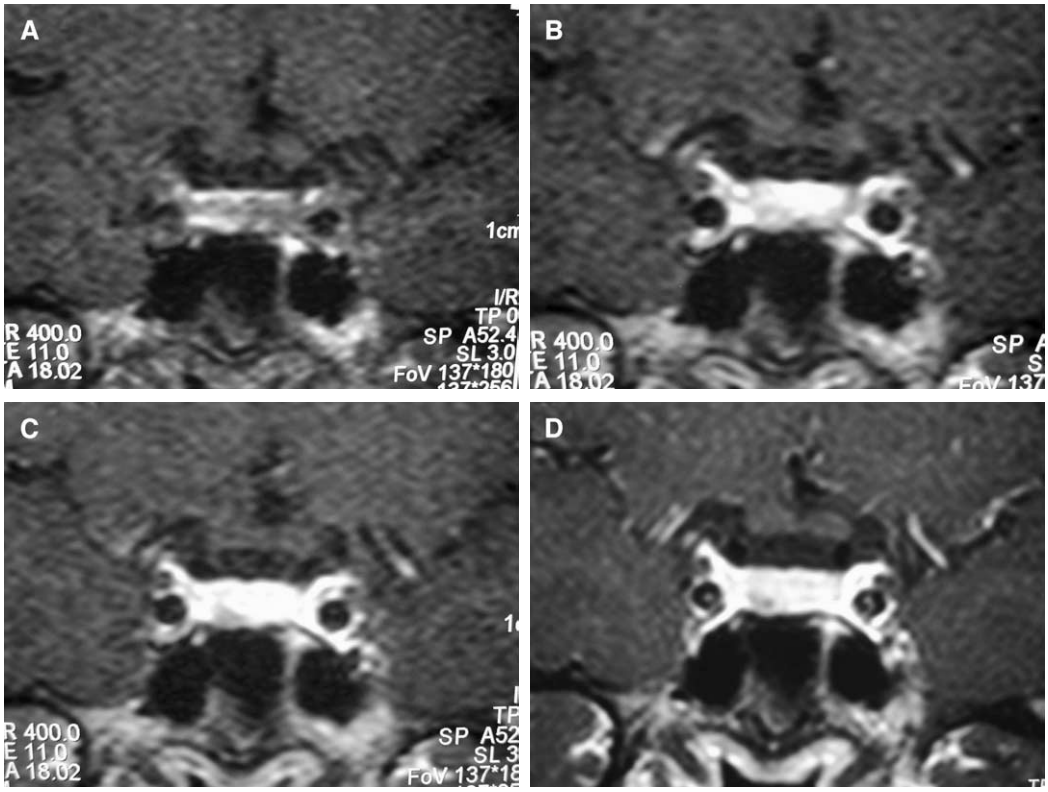

Fig. 2. Dynamic sellar MRI study for pituitary microadenoma. (*A*) Coronal dynamic postcontrast image obtained 20 seconds after injection of contrast material demonstrates a focal area of contrast enhancement over the right inferior aspect of the pituitary gland. (*B*) Coronal dynamic postcontrast image obtained 40 seconds after injection demonstrates a focal area of decreased contrast enhancement over the right inferior aspect of the pituitary gland, which begins to show intense enhancement. (*C*) Coronal dynamic postcontrast image obtained 80 seconds after injection demonstrates a focal area of decreased contrast enhancement over the right inferior aspect of the enhancing pituitary gland. (*D*) Coronal postcontrast T1-weighted image demonstrates a focal area of decreased contrast enhancement over the right inferior aspect of the pituitary, which is consistent with a microadenoma.

small adenomas; in one series, all the adenomas discovered measured less than 4 mm in size [10]. Histologically, pituitary adenomas are monomorphic in cellular appearance but with variable tinctorial properties [12]. There are three types of histopathologic profiles for pituitary adenomas, namely, sinusoidal, diffuse, and papillary. In general, tumors of the pituitary tend to be hypovascular compared with the normal pituitary gland. Areas of cystic and necrotic degeneration, fibrosis, and infarction are seen [11]. Calcification was seen in 7% of cases in one of the surgical series [13].

The most common pituitary adenomas are prolactinomas, comprising approximately 30% to 40% of all pituitary tumors. Prolactinomas are predominantly seen in women with a 5:1 female-to-male ratio [14]. In young women, they often present with amenorrhea and galactorrhea, whereas in postmenopausal women and men, they often cause loss of libido, mood swings, and headache [15]. Prolactinomas are associated with significant elevation of prolactin levels, usually more than 150 ng/mL. A prolactin level of less than 100 ng/mL may be caused by various pathologic findings, including hypothalamic compression, hypothalamic mass, and drug-induced hyperprolactinemia.

Nonfunctioning adenomas are the second most common tumors, comprising 25% of pituitary adenomas [12]. These tumors often grow to a significant size and cause optic chiasmal compression or other mass effect before they are detected.

ACTH-secreting tumors and growth hormone–secreting tumors account for less than 10% of pituitary tumors. Thyroid-stimulating hormone adenomas account for 1% to 4% of pituitary tumors [12,16]. ACTH-secreting adenomas are usually small when detected because of their potent endocrinologic effects.

Most pituitary adenomas are microadenomas (less than 1 cm in diameter), and they usually present with endocrine effects. Macroadenomas (greater than 1 cm in diameter) are either nonsecretory tumors or endocrinologically inapparent. They usually present with headache, hydrocephalus, and visual loss. Macroadenomas can reach a significant size before they become clinically symptomatic. Extension of the pituitary tumor into the cavernous sinus can be difficult to appreciate. A definitive diagnosis can only be made when the cavernous portion of the internal carotid artery is encircled by the tumor or when the lateral wall of the cavernous sinus is convex [4].

Imaging features

CT

Pituitary adenomas are isodense to adjacent brain parenchyma on unenhanced CT. They demonstrate intense contrast enhancement after injection of contrast material. Bony erosion and expansion of the sellar turcica are well demonstrated on bone window images. Calcification is uncommon (5%). Hemorrhage within the pituitary tumor is uncommon and can be detected as focal hyperdensity.

MRI

Diagnosis of pituitary microadenomas is a challenge. Microadenomas are commonly hypointense to the pituitary gland on T1-weighted images and usually enhance less than the normal pituitary gland; however, they may occasionally show more intense enhancement. Their appearance on T2-weighted images is variable [17]. On dynamic contrast-enhanced studies, most of these tumors show enhancement before the pituitary gland; later on, the tumor enhancement begins to wash out, whereas the pituitary begins to show enhancement. Therefore, pituitary microadenomas usually show less contrast enhancement compared with the adjacent pituitary gland. Secondary signs of pituitary microadenoma include deviation of the pituitary stalk and bulging of the superior or inferior margin of the gland (Fig. 3). Macroadenomas are usually hypointense to isointense to gray matter on T1-weighted images and variable in signal intensity on T2-weighted images. Large macroadenomas are usually easy to diagnose on coronal postcontrast images and are seen as enhancing masses (Fig. 4). Bony erosion by the tumor mass causes the sellar turcica to enlarge. Tumors may show infrasellar extension into the

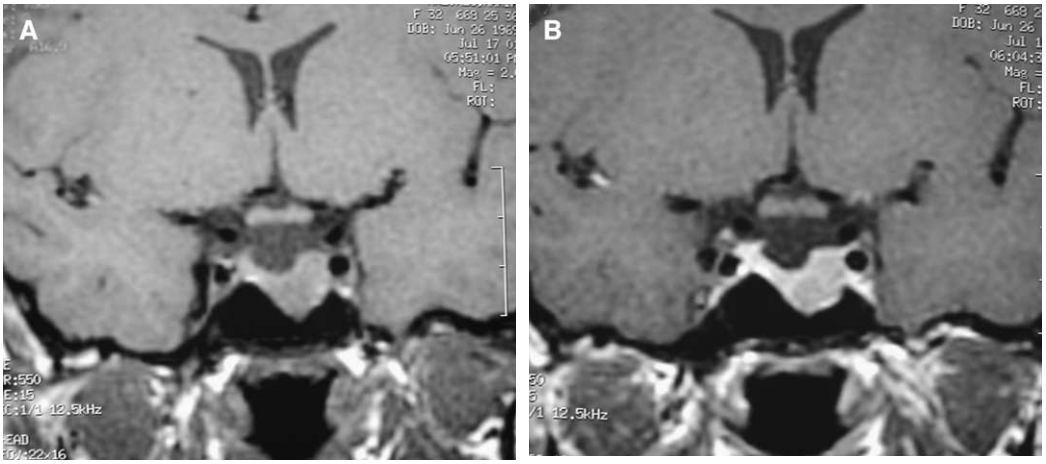

Fig. 3. Pituitary microadenoma (prolactinoma). (*A*) Coronal T1-weighted image shows a focal mass on the left side of the pituitary gland with remodeling of the floor of the sellar turcica on the left side as well as superior convexity of the upper margin. (*B*) Coronal postcontrast T1-weighted image shows decreased enhancement of the mass compared with the pituitary.

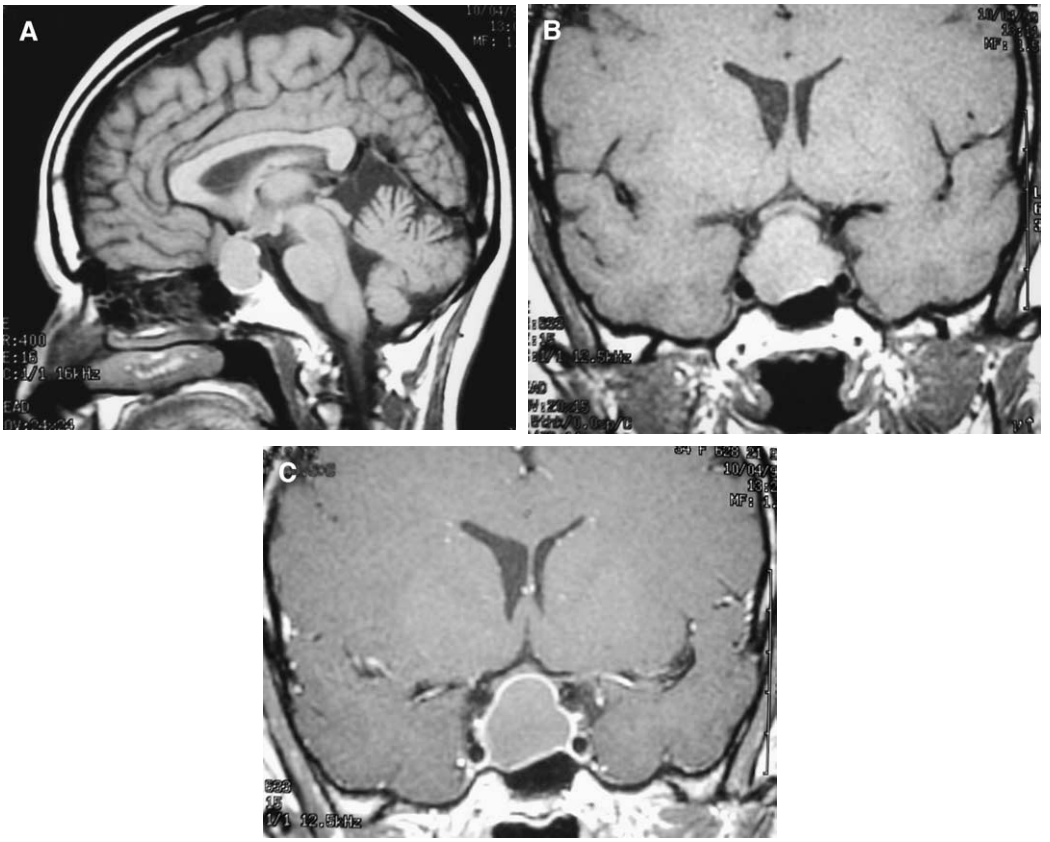

Fig. 4. Pituitary macroadenoma. (*A*) Sagittal T1-weighted image show a large isointense mass in the enlarged sellar turcica with suprasellar and infrasellar extension. (*B*) Coronal T1-weighted image demonstrates a large sellar mass with suprasellar extension and compression of the optic chiasm. The mass appears to extend into the cavernous sinuses bilaterally. Infrasellar extension of the mass into the sphenoid sinus is also seen. (*C*) Coronal postcontrast T1-weighted image demonstrates enhancement of the mass as well as enhancement of the peripheral rim.

sphenoid sinus, suprasellar extension with optic chiasmal compression, and parasellar extension with encirclement of the carotid arteries (Figs. 5 and 6) [18]. Dural enhancement at the planum sphenoidale and carotid sulcus may be seen [19]. Asymmetric tentorial enhancement can be a useful sign in the diagnosis of invasion or severe compression of the cavernous sign by pituitary tumor. This sign may be explained by venous congestion in the tentorium secondary to obstructed flow in the cavernous sinus [20]. Hemorrhage of the adenoma is seen as high signal intensity on T1-weighted images. Intratumoral hemorrhage may be seen without clinical evidence of apoplexy [21]. Although rare, subarachnoid dissemination in postoperative pituitary adenomas has been reported [22].

It is important to recognize the usual postoperative changes in the sella after transsphenoidal surgery for a pituitary adenoma [23,24]. The late postoperative findings include the re-expansion of the normal pituitary gland, thickening of the pituitary stalk, swelling of the optic chiasm, and resorption of the implanted material. Several reports on CT and MRI in the early postoperative studies demonstrated a lack of change in the overall size of the pituitary mass immediately after surgery. Follow-up CT or MRI studies have shown a significant decrease in the size of the pituitary mass 3 or 4 months after surgery [25,26]. There are several explanations for this phenomenon, including resorption of the packing, overpacking of the tumor bed, postoperative

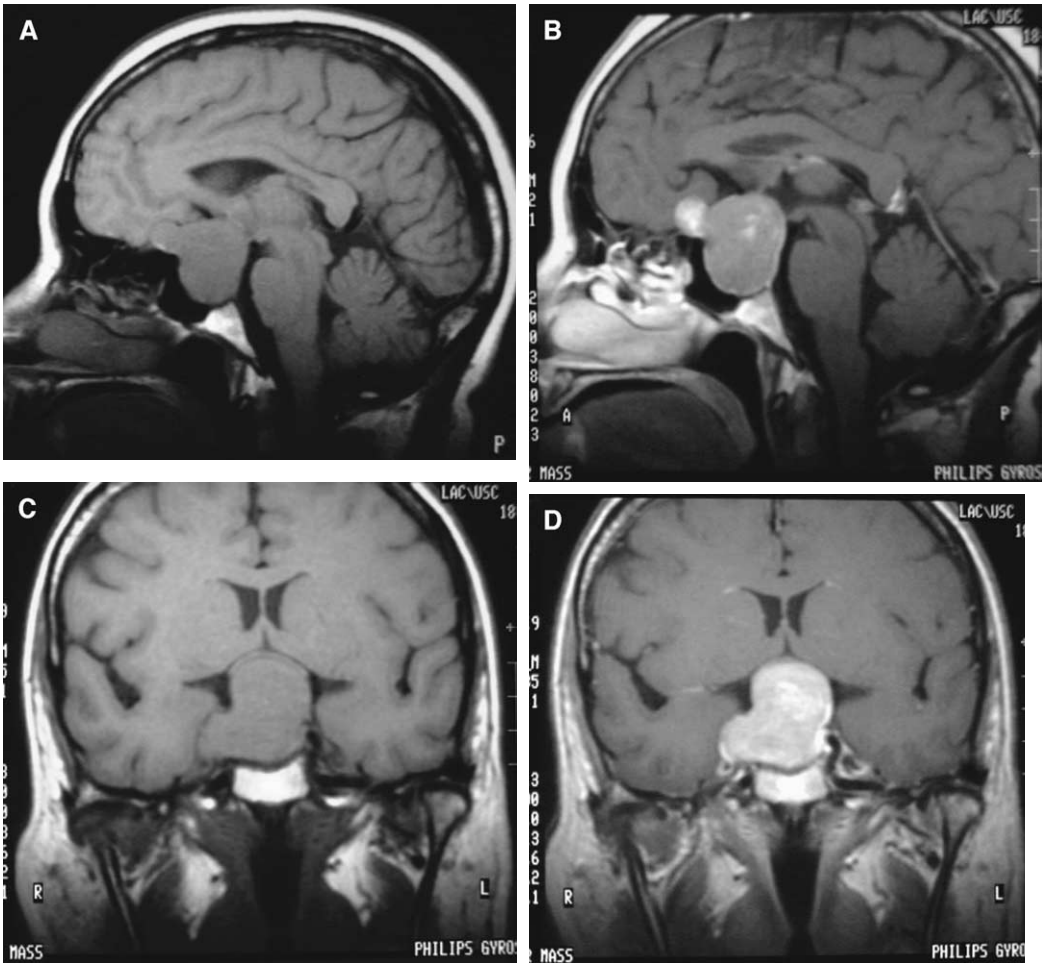

Fig. 5. Macroadenoma. (*A*) Sagittal T1-weighted image shows a large isointense sellar mass with suprasellar extension, which extends into the subfrontal region. The optic chiasm is markedly compressed and cannot be identified. Remodeling of the floor of the sellar turcica is also seen. (*B*) Sagittal postcontrast T1-weighted image demonstrates enhancement of the large mass lesion, with more enhancement seen in the subfrontal component. (*C*) Coronal T1-weighted image shows a large mass with suprasellar extension and marked compression of the optic chiasm. Extension of the mass into the right cavernous sinus is also seen. (*D*) Coronal postcontrast T1-weighted image shows enhancement of the large sellar mass.

hemorrhage, residual tumor or tumor capsule, and adhesions. Early postoperative dynamic MRI after transsphenoidal surgery for a pituitary macroadenoma may be useful in differentiating residual tumor from postoperative changes [27].

Pituitary hyperplasia

Primary hypothyroidism can cause pituitary hyperplasia and mimic a pituitary macroadenoma. In this case, the history of hypothyroidism is important in making the correct diagnosis. Pituitary hyperplasia in these patients can regress after treatment with thyroxine for hypothyroidism [28].

Craniopharyngioma

Craniopharyngiomas account for approximately 3% to 5% of all intracranial tumors,

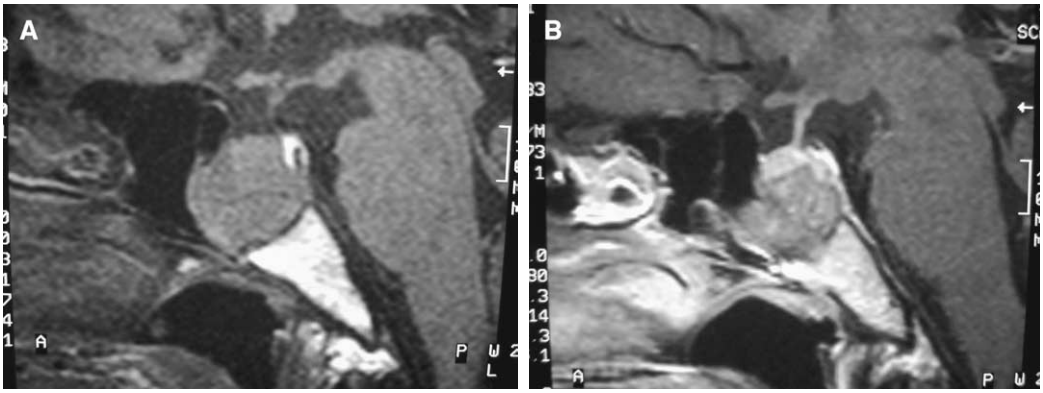

Fig. 6. Macroadenoma with infrasellar location. (*A*) Sagittal T1-weighted image shows a large mass in the infrasellar location. The normal pituitary is seen at the superior aspect of the mass. (*B*) Sagittal postcontrast T1-weighted image demonstrates the mass in an infrasellar sphenoid sinus location. The normal pituitary is seen at the superior aspect of the mass and shows slightly more intense enhancement compared with the macroadenoma.

5% to 10% of all pediatric intracranial neoplasms, 15% of supratentorial tumors, and 50% of suprasellar tumors in children. Craniopharyngiomas have a bimodal age distribution; most occur in children and young adults [29]. A second much smaller peak is seen in fifth and sixth decades. Male and female patients are equally affected. Craniopharyngiomas are both intrasellar and suprasellar in approximately 70% of cases, suprasellar only in 20% of cases, and intrasellar in nearly 10% of cases. Fewer than 1% arise within an anterior third ventricle. They are thought to derive from either metaplastic adenohypophyseal cells or Rathke's pouch remnants [12]. Clinically, they usually present with headache, visual problems, hydrocephalus, and endocrine disorders, including diabetes insipidus and growth deficiency. The histopathologic findings of pediatric craniopharyngiomas consist of adamantinomatous epithelium, keratin nodule formation, and prominent cholesterol-filled cyst formation. Calcification is common in adamantinomatous craniopharyngioma (90%). These tumors often have cystic and solid components. The cystic portions consist of an outer epithelial cell layer on a collagenous basement membrane. Cyst contents range from straw-colored fluid to a crankcase oil–like mixture of keratin, cholesterol, protein, necrotic debris, and blood products [30].

In one third of the adult type lesions, a papillary histologic type is seen [31]. They usually do not exhibit calcification or cystic components and behave in a less aggressive manner. A mixed histologic pattern of the adamantinomatous and papillary types is also seen.

Spontaneous intraventricular rupture of cystic craniopharyngioma is rare but has been reported [32]. The intraventricular rupture of a cystic craniopharyngioma can result in acute clinical deterioration because of chemical ventriculitis and meningitis. Craniopharyngiomas are usually histologically benign, although they may be locally aggressive, and tend to recur after surgery. Malignant change in craniopharyngiomas is extremely rare. The transition of typical craniopharyngioma to squamous cell carcinoma has been well documented [33]. Recurrence of craniopharyngioma at an ectopic location is well documented [34,35].

Imaging features

CT

Craniopharyngiomas are well-circumscribed multiloculated masses, 90% of which have both cystic and solid components. The cystic portions typically have a density approximating that of cerebrospinal fluid (CSF) but may be hypodense in proportion to cholesterol content and hyperdense in proportion to proteinaceous content. Calcification is seen in 70% to 90% of these patients and is more commonly seen in children. Solid portions, nodules, and cyst walls enhance in response to contrast material injection [36]. Intraventricular rupture of craniopharyngio-

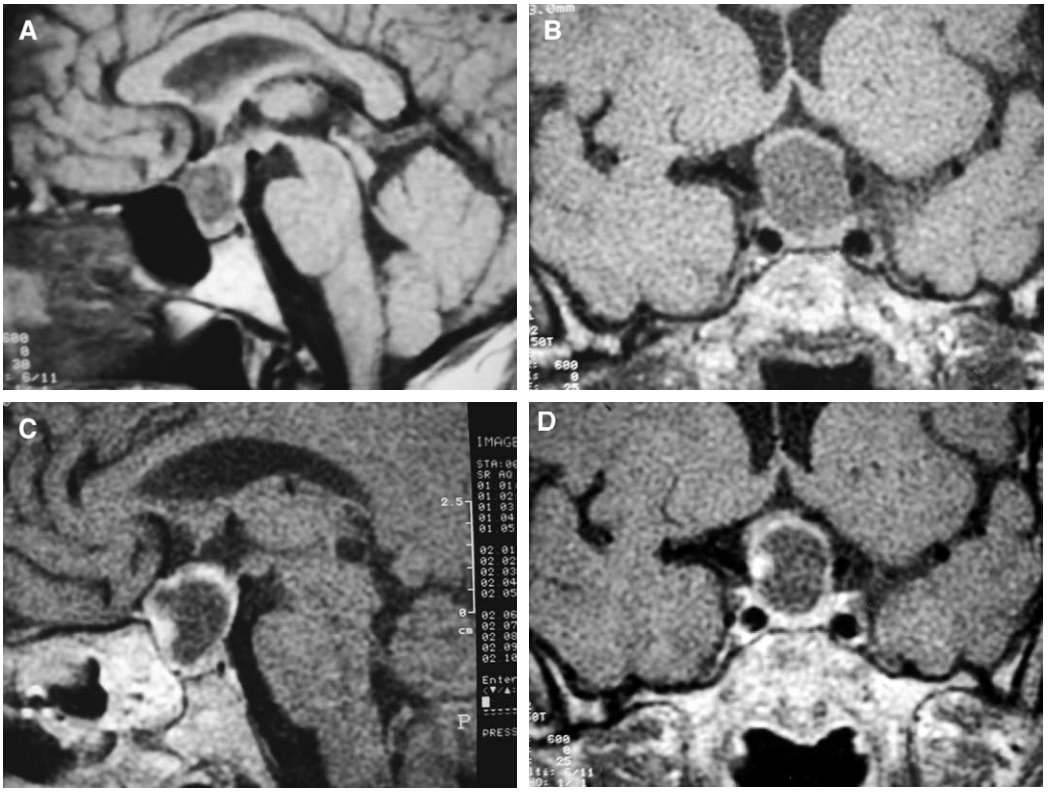

Fig. 7. Craniopharyngioma. (*A*) Sagittal T1-weighted image shows a cystic mass in the suprasellar region. (*B*) Coronal T1-weighted image shows a large cystic mass in the suprasellar region with compression of the optic chiasm. (*C*) Coronal postcontrast T1-weighted image shows enhancement of the irregular cyst wall. (*D*) Sagittal postcontrast T1-weighted image demonstrates enhancement of the cyst wall with a nodular area on the right side.

mas may demonstrate a fluid-fluid level in the occipital horns of the lateral ventricle.

MRI

The signal characteristics of the cystic component of craniopharyngiomas are highly variable: hyperintensity correlates with high protein or methemoglobin content on T1-weighted images, but T2-weighted images are more typically hyperintense [37-39]. The solid component is hypointense to isointense on T1-weighted images and hyperintense on T2-weighted images. Avid but heterogeneous enhancement of the solid component and cyst wall is seen (Figs. 7 and 8) [31]. Intraventricular rupture of craniopharyngiomas may demonstrate a fluid-fluid level in the occipital horns of the lateral ventricle.

Rathke's cleft cyst

Rathke's cleft cysts are common, but most are microscopic and not visible on imaging studies. On imaging studies, they are cystic lesions in the sellar or suprasellar region with compression of the pituitary stalk or hypothalamus. Pathologically, the cyst walls are composed of squamous, cuboidal, or pseudostratified columnar epithelium, occasionally with goblet cells or even mucus glands. The cyst fluid may show variable signal intensity on T1-weighted images depending on the content of the cyst fluid (Fig. 9). The cyst wall is usually thin, but a thickened wall with calcification may occasionally be seen. Mild contrast enhancement may be seen. Rarely, hemorrhage can occur in these cysts, mimicking pituitary apoplexy [40].

Arachnoid cyst

Suprasellar arachnoid cysts are predominantly seen in children younger than 5 years of age, but, they may occasionally be seen in young adults [41,42]. Clinical symptoms include increased intracranial pressure, spasticity, gait disturbance, and

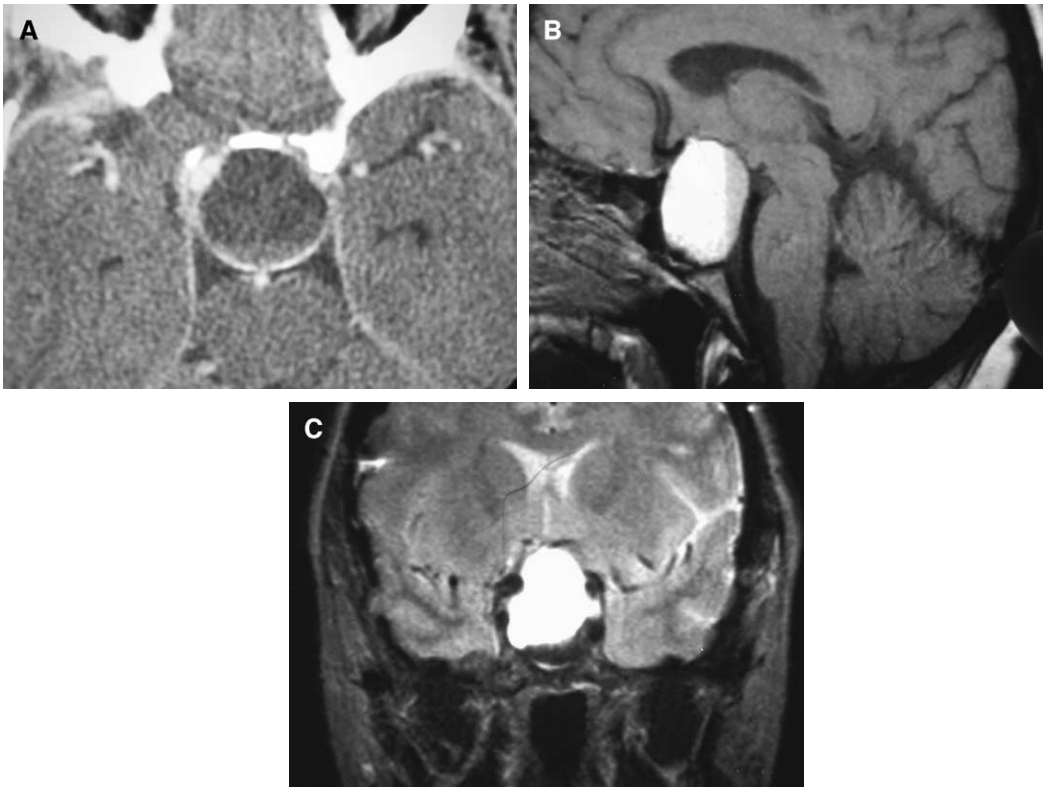

Fig. 8. Craniopharyngioma. (*A*) Axial postcontrast CT scan shows a cystic mass with rim enhancement in the suprasellar region. (*B*) Sagittal T1-weighted image shows a large cystic mass involving the sellar and suprasellar regions. The mass shows high signal intensity on T1-weighted imaging, consistent with high protein content. A fluid-fluid level is seen within the cystic lesion. (*C*) Coronal T2-weighted image demonstrates a high signal intensity mass with suprasellar extension and slight parasellar extension into the cavernous sinuses.

visual problems. On MRI, a CSF signal intensity mass with focal mass effect is seen. The cyst membrane is usually not well defined [43].

Epidermoid

Epidermoids are developmental epithelial inclusion cysts. They are commonly seen in the cerebellopontine angle cisterns and suprasellar cistern. They consist of less than 2% of all intracranial neoplasms and are seen in patients from 30 to 60 years of age. These masses are usually isointense to CSF on both T1-weighted and T2-weighted images (Fig. 10) [44,45]. Some heterogeneity is sometimes seen with a "dirty CSF" appearance. The cholesterol content within the epidermoid is not hydrolyzed and therefore does not exhibit high signal intensity on T1-weighted images. The cyst wall consists of stratified squamous epithelium, and desquamation of the epithelial lining contributes to the cellular debris, keratin, and cholesterol crystals seen within the cyst.

Empty sella

Extension of the subarachnoid space of variable size with herniation of the arachnoid through an incompetent diaphragma sellae is called empty sella, and it does not usually have any clinical significance. The pituitary gland is flattened and displaced toward the posterior inferior aspect of the pituitary fossa. CT and MRI demonstrate an enlarged sella turcica filled with CSF density or signal intensity. The infundibulum is normal in its course and inserts into the flattened gland. Empty sella can also occur in postsurgical cases or in cases

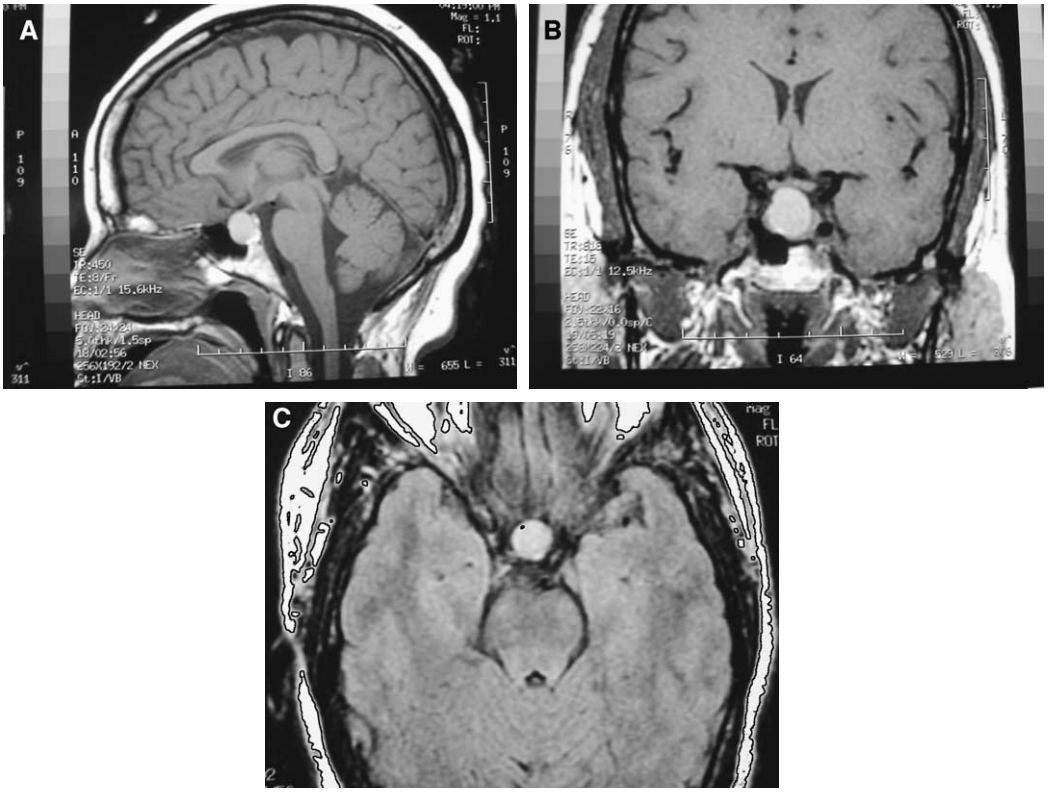

Fig. 9. Rathke's cleft cyst. (*A*) Sagittal T1-weighted image shows a hyperintense mass in the sella with slight suprasellar extension. (*B*) Coronal T1-weighted image shows a hyperintense mass with suprasellar extension, which appears to encroach on the optic chiasm. (*C*) Axial T2-weighted image shows the mass to be hyperintense as well.

of previous adenohypophysitis. Sheehan's syndrome can also result in an acquired empty sella.

Hypothalamic astrocytoma

Hypothalamic-chiasmatic astrocytomas are primarily masses seen in childhood and are rarely documented in adulthood [46]. Astrocytomas arising from the hypothalamus, optic chiasm, optic nerve, and optic tract account for approximately 30% of neoplasms in childhood. These lesions are often difficult to delineate between locations in the hypothalamus versus the optic chiasm; hence, they are often referred to in the literature as hypothalamic-chiasmatic gliomas [47]. The main subtype of astrocytomas seen by histopathologic testing in this region during childhood is the juvenile pilocytic astrocytoma, a low-grade lesion. A significant number of these lesions (approximately 33%) are associated with the neurocutaneous syndrome–neurofibromatosis type I. When associated with this syndrome, other lesions may be seen, including optic nerve gliomas; low-grade brain stem gliomas; and non-neoplastic hamartomas in the basal ganglia, white matter, and dentate nucleus. Given the location of these lesions, various clinical presentations are seen, including visual abnormalities, diabetes insipidus, sexual precocity, obesity, emaciation, hyperactivity, and euphoria [48,49].

Imaging features

CT

CT usually demonstrates a hypodense to isodense mass before the injection of contrast material. On postcontrast images, there is variable enhancement of the mass lesion seen. These lesions rarely demonstrate calcification or hemorrhage. Although they are pilocytic astrocytomas

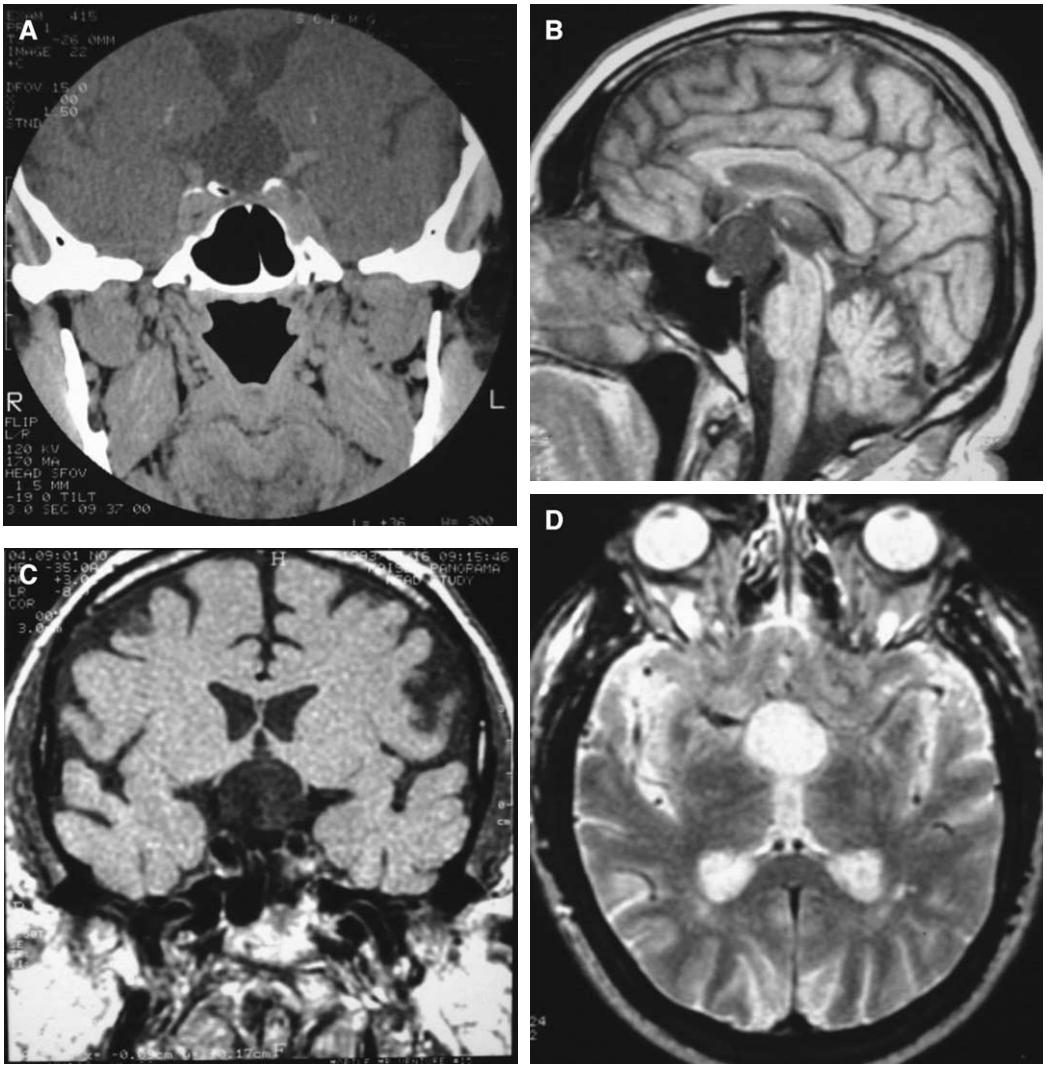

Fig. 10. Epidermoid. (*A*) Coronal postcontrast CT scan demonstrates a cystic suprasellar mass with no evidence of enhancement. (*B*) Sagittal T1-weighted image demonstrates a cystic suprasellar mass with compression of the optic chiasm. The mass shows similar signal intensity as cerebrospinal fluid (CSF). (*C*) Coronal T1-weighted image demonstrates suprasellar cystic mass with compression of the optic chiasm. (*D*) Axial T2-weighted image reveals the cystic mass with similar signal intensity to CSF.

histologically, they are usually solid lesions. Occasionally, small cystic or necrotic components can be seen in large lesions.

MRI

On MRI, these lesions are usually hypointense on T1-weighted images and hyperintense on T2-weighted images. Again, as on CT, there usually is variable enhancement after contrast administration (Fig. 11). These imaging findings are by no means exclusive to hypothalamic-chiasmatic gliomas; when they are visualized, other disease processes should be entertained as diagnostic possibilities. These considerations include but are not limited to sarcoidosis, Langerhans cell histiocytosis, germinoma, metastasis, and lymphoma. It is often the case with these lesions that biopsy is necessary to make the final diagnosis.

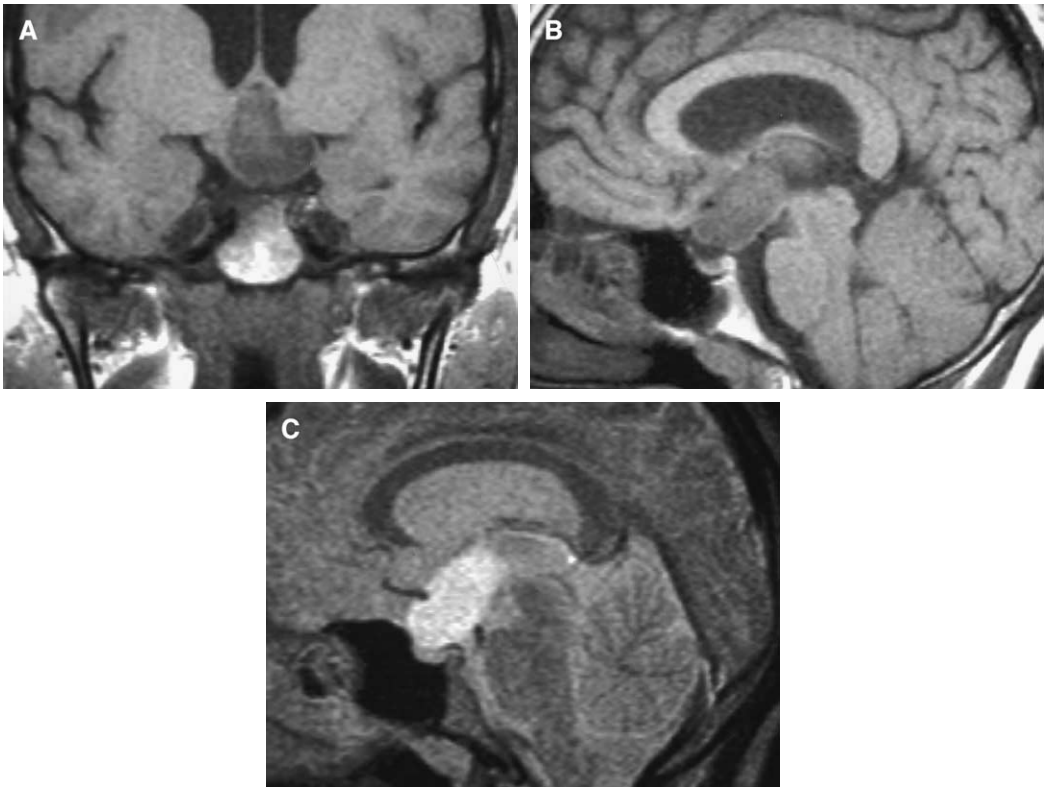

Fig. 11. Hypothalamic astrocytoma. (*A*) Coronal T1-weighted image shows a hypointense mass in the suprasellar region. The optic chiasm is displaced inferiorly. (*B*) Sagittal T1-weighted image shows a hypointense mass in the suprasellar region. The optic chiasm is seen displaced inferiorly. (*C*) Sagittal T2-weighted image shows a hyperintense mass in the suprasellar region. The normal pituitary can be seen inferior to the mass.

Meningioma

Meningioma is the most common nonglial primary brain tumor and the most common intracranial extra-axial neoplasm, comprising 15% of primary brain tumors [29]. The peak incidence of meningiomas occurs between the ages of 40 and 70 years; they are rare in children, comprising 1% to 2% of all pediatric brain tumors. There is a strong association of meningioma with neurofibromatosis. There is a female-to-male ratio of 2:1. Approximately 5% to 10% of meningiomas arise from the sellar region. Meningioma in the sellar region can arise from the diaphragma sellar, tuberculum sellar, planum sphenoidale, medial lesser wing of sphenoid, anterior clinoid, clivus, cavernous sinus, or optic nerve sheath. Suprasellar meningiomas usually arise from the diaphragma sellae or tuberculum sellae. Rarely, meningiomas can occur entirely within the sella turcica, mimicking a pituitary adenoma [50].

Imaging features

CT

On noncontrast CT scans, meningiomas appear as sharply circumscribed extra-axial tumors of slight hyperdensity. Calcification is seen in 20% to 50% of cases and may be diffuse or focal, appearing in psammomatous, sunburst, globular, or ring-like patterns. Intense enhancement is seen after intravenous injection of contrast material.

MRI

Like meningiomas elsewhere, they are usually seen as isointense to gray matter on both T1-weighted and T2-weighted images, although T2 signal intensity may be more variable. Avid enhancement is usually seen after the intravenous injection of contrast (Figs. 12 and 13). Meningiomas can usually be separated from the pituitary gland because of their differential enhancing

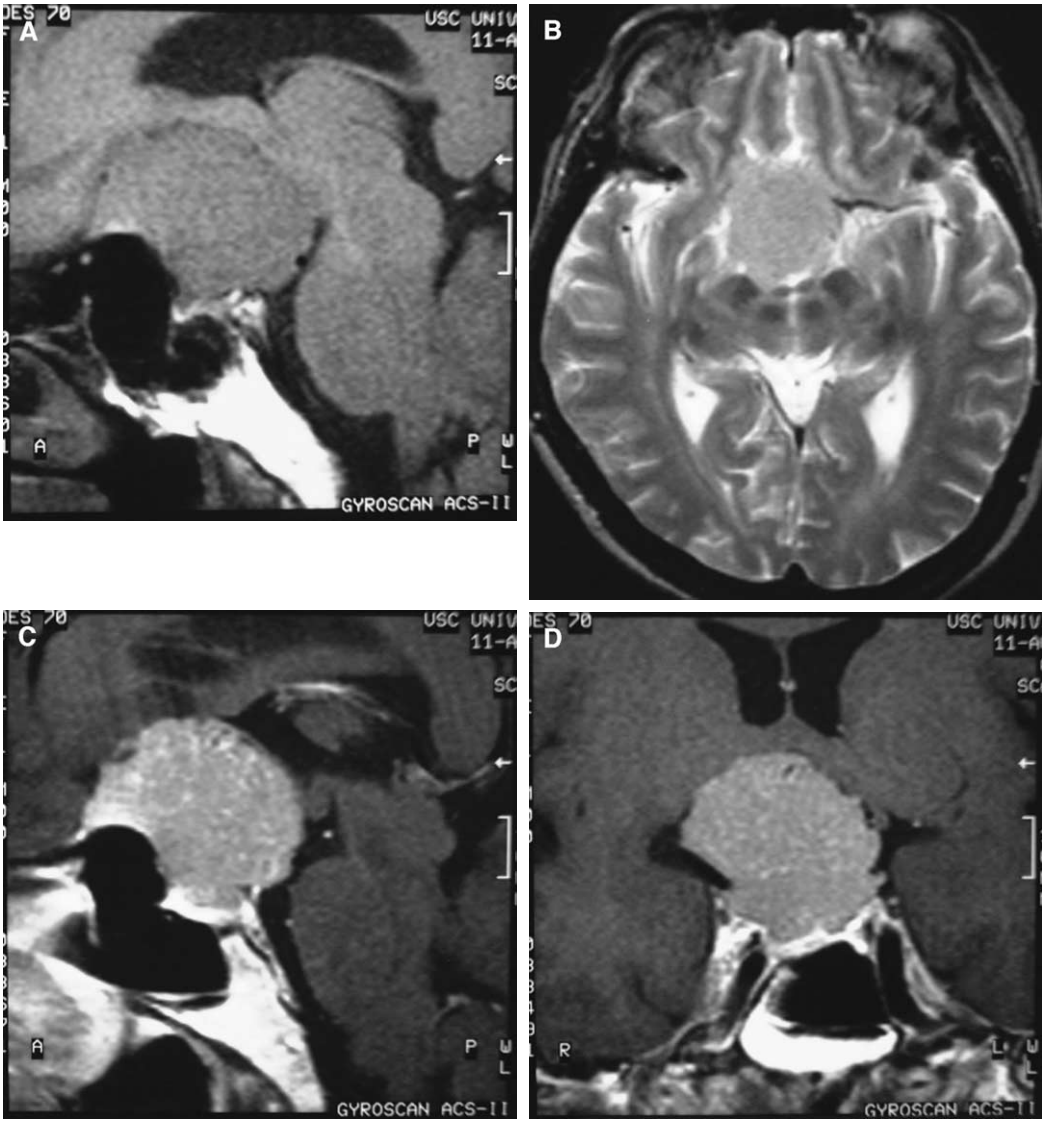

Fig. 12. Suprasellar meningioma. (*A*) Sagittal T1-weighted image shows a large suprasellar isointense mass with subfrontal extension. (*B*) Axial T2-weighted image shows the mass to be isointense to gray matter. (*C*) Sagittal postcontrast T1-weighted image shows homogeneous enhancement of the mass. The pituitary gland is seen inferior to the mass and demonstrates more contrast enhancement. (*D*) Coronal postcontrast T1-weighted image demonstrates enhancement of the suprasellar mass.

pattern. They can invade the cavernous sinus with encasement of the internal carotid arteries. Most of the meningiomas have dural attachment and show a dural tail on the postcontrast imaging studies. A few rare cases of meningiomas originating from the pituitary stalk without dural attachment have been reported in the literature [51].

Hemangiopericytoma

Hemangiopericytoma is an aggressive and highly vascular neoplasm that arises from vascular pericytes. Macroscopically, they resemble meningiomas and used to be grouped with ''angioblastic meningiomas.'' They are well-

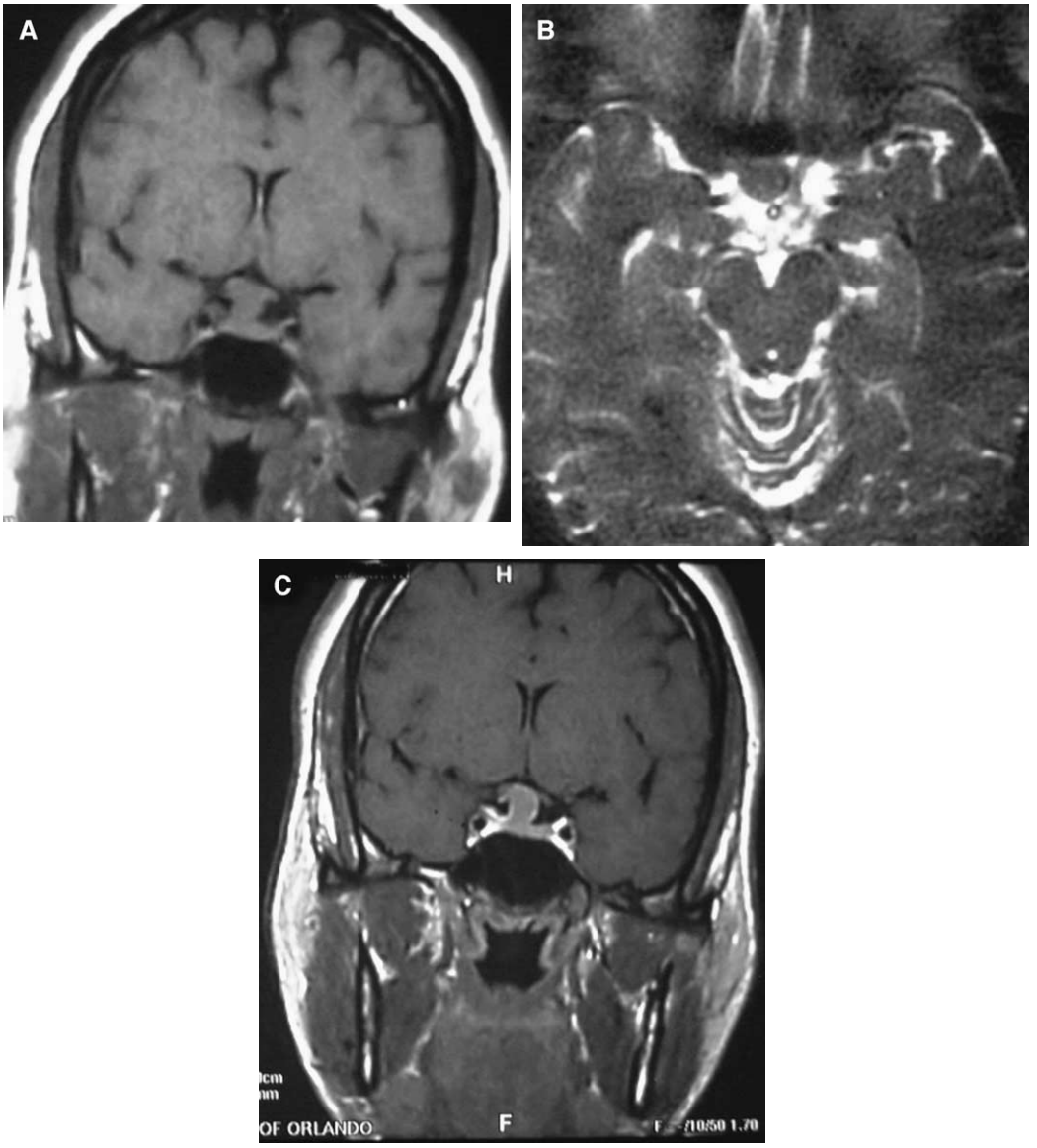

Fig. 13. Small suprasellar meningioma. (*A*) Coronal T1-weighted image shows a small isointense suprasellar mass between the optic chiasm and pituitary gland. (*B*) Axial T2-weighted image shows the mass to be isointense to gray matter. (*C*) Coronal postcontrast T1-weighted image shows an enhancing mass in the suprasellar region with compression of the optic chiasm. Note that the mass has similar enhancement as the pituitary gland.

circumscribed masses with numerous penetrating vessels. Microscopically, they have a dense pervasive reticular network with lobules and neoplastic cells. Similar to optic meningioma, they can arise from the optic nerve sheath or cavernous sinus. They can present as sellar and suprasellar masses, mimicking pituitary adenoma [52,53]. Local tumor recurrence after treatment with surgery and radiation is common, and late and widespread metastasis can occur. On MRI, they appear hypointense on T1-weighted images and heterogeneously hyperintense on

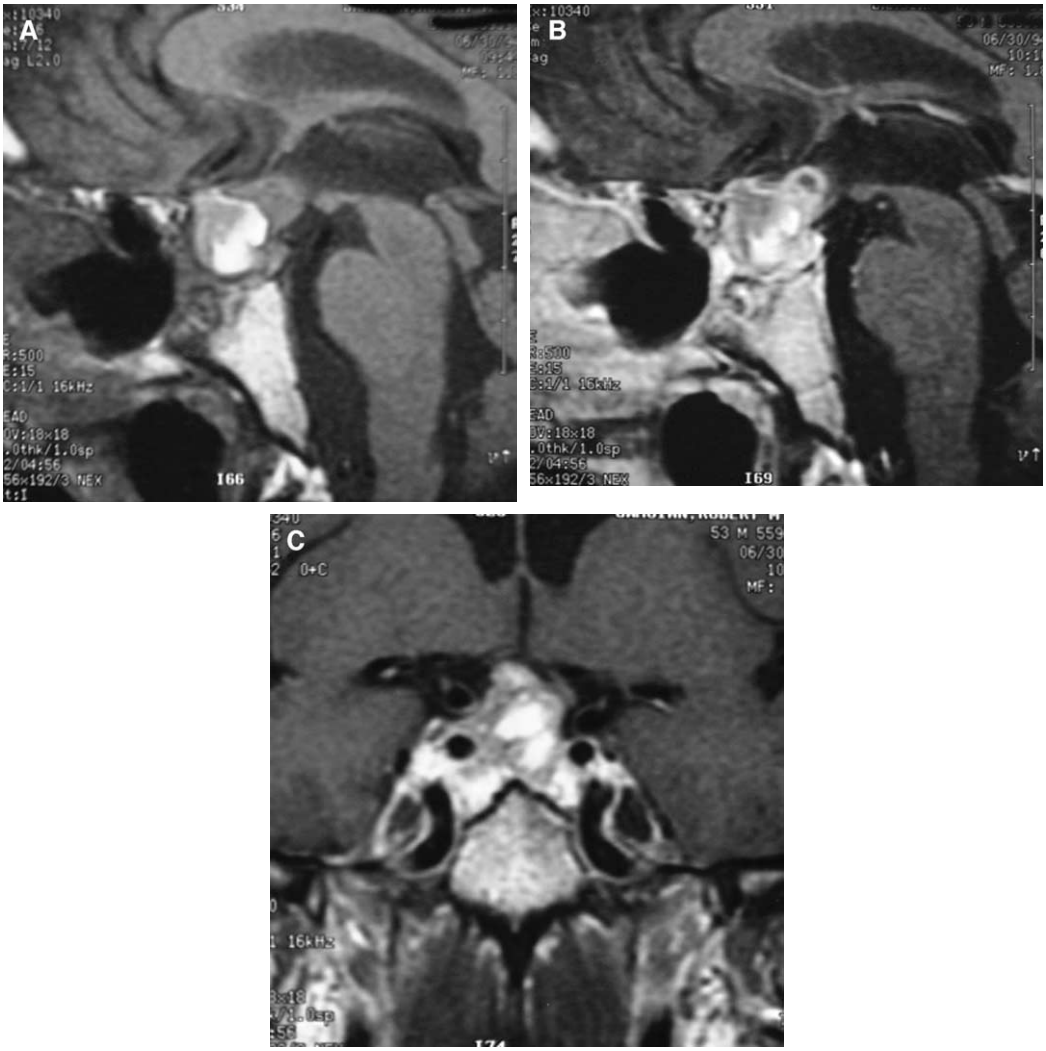

Fig. 14. Hemangiopericytoma. (*A*) Sagittal T1-weighted image shows a sellar suprasellar mass with mixed signal intensity. Areas of hyperintensity are probably caused by focal hemorrhage. (*B*) Sagittal postcontrast T1-weighted image demonstrates irregular enhancement of the mass lesion. (*C*) Coronal postcontrast T1-weighted image demonstrates irregular enhancement of the mass with suprasellar extension and right parasellar extension into the cavernous sinus. Note that the mass surrounds the right internal carotid artery completely.

T2-weighted images. Cystic and necrotic areas, hemorrhage, and prominent vascular channels contribute to the heterogeneity in signal intensity (Fig. 14).

Schwannoma

Nerve sheath tumors in the parasellar region usually arise from the Gasserian ganglion in Meckel's cave [54,55]. Schwannomas of the third, fourth, and sixth cranial nerves are rare [56]. Expansion of the cavernous sinus with convexity of the lateral wall of the cavernous sinus can be identified. Bony remodeling of the lateral portion of the sellar turcica may be seen. CT shows a hypodense to isodense mass with intense contrast enhancement. On MRI, they are hypointense on T1-weighted images and hyperintense on T2-weighted images. Avid enhancement is seen after the intravenous injection of contrast material (Fig. 15).

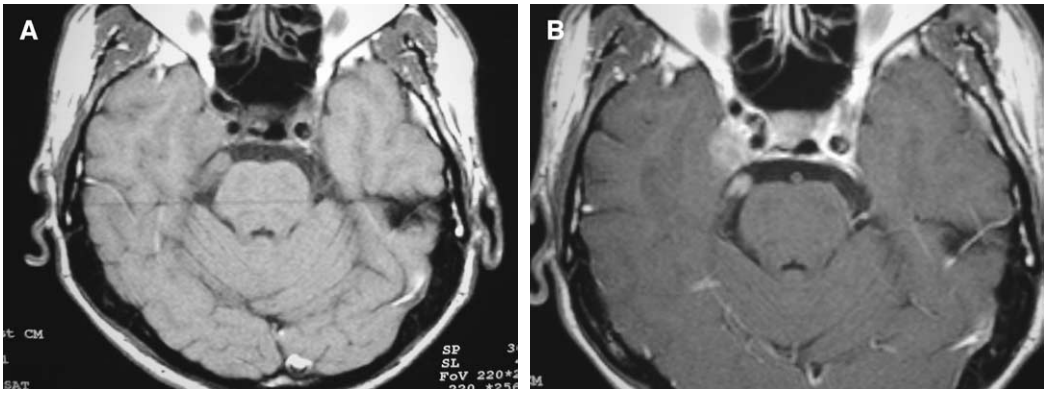

Fig. 15. Right parasellar fifth nerve schwannoma. (*A*) Axial T1-weighted image shows an isointense mass involving the right cavernous sinus and along the right fifth cranial nerve. (*B*) Axial postcontrast image shows enhancement of the mass lesion.

Germinoma

Intracranial germinomas occur most frequently in the pineal region. The suprasellar region is the second most common site for germinomas. Germinomas in the suprasellar region are seen equally in men and women, whereas germinomas in the pineal region are seen almost exclusively in men [57]. Suprasellar germinomas are seen in young adult patients, often with visual or endocrine disorders, such as diabetes insipidus [58]. Suprasellar germinomas are usually isointense to gray matter on T1-weighted images and slightly hyperintense on T2-weighted images. The tumor mass enhances homogeneously after intravenous injection of contrast. Suprasellar germinoma may be seen with germinoma in the pineal region in the same patient (Fig. 16).

Mixed malignant germ cell tumors may show heterogenous signal intensity and heterogeneous enhancement (Fig. 17). The presence of tumor markers, such as α-fetoprotein or β-human chorionic gonadotropin, in the CSF or blood may assist in the diagnosis.

Metastasis

Metastatic tumor to the pituitary is uncommon, occurring in 3% of patients dying of cancer as determined during autopsy [12]. Metastatic tumor to the parasellar region can occur in the cavernous sinus, clivus, or sphenoid bone. Common sites of primary cancer include the breast, lung, prostate, colon, and melanoma. Metastases tend to occur in the pituitary stalk and posterior pituitary initially and to spread to the anterior pituitary later. The hypophysis, infundibulum, and tuber cinereum are more susceptible to hematogenous metastasis because of the absence of blood–brain barrier in these areas (Fig. 18).

Pituitary abscess

Purulent acute adenohypophysis is rare. Predisposing symptoms include sepsis, sinusitis, sphenoid osteomyelitis, cavernous sinus thrombophlebitis, meningitis, and the postoperative state after pituitary removal. Occasionally, a pituitary abscess can arise in preexisting pathologic features, such as a pituitary adenoma or a Rathke's cleft cyst [59,60]. CT or MRI shows a cystic sellar mass with ring-like enhancement. A pituitary abscess may progress slowly and may allow remodeling of the sella to occur.

Tuberculosis

Tuberculosis of the pituitary gland is rare. It may result from direct extension from tuberculous meningitis or through hematogenous spread. MRI shows a pituitary mass similar to pituitary adenoma [61].

Sarcoidosis

Sarcoidosis of the central nervous system has a predilection for the leptomeninges, although other areas, such as the hypothalamus, optic chiasm, and pituitary stalk, may be involved (Fig. 19).

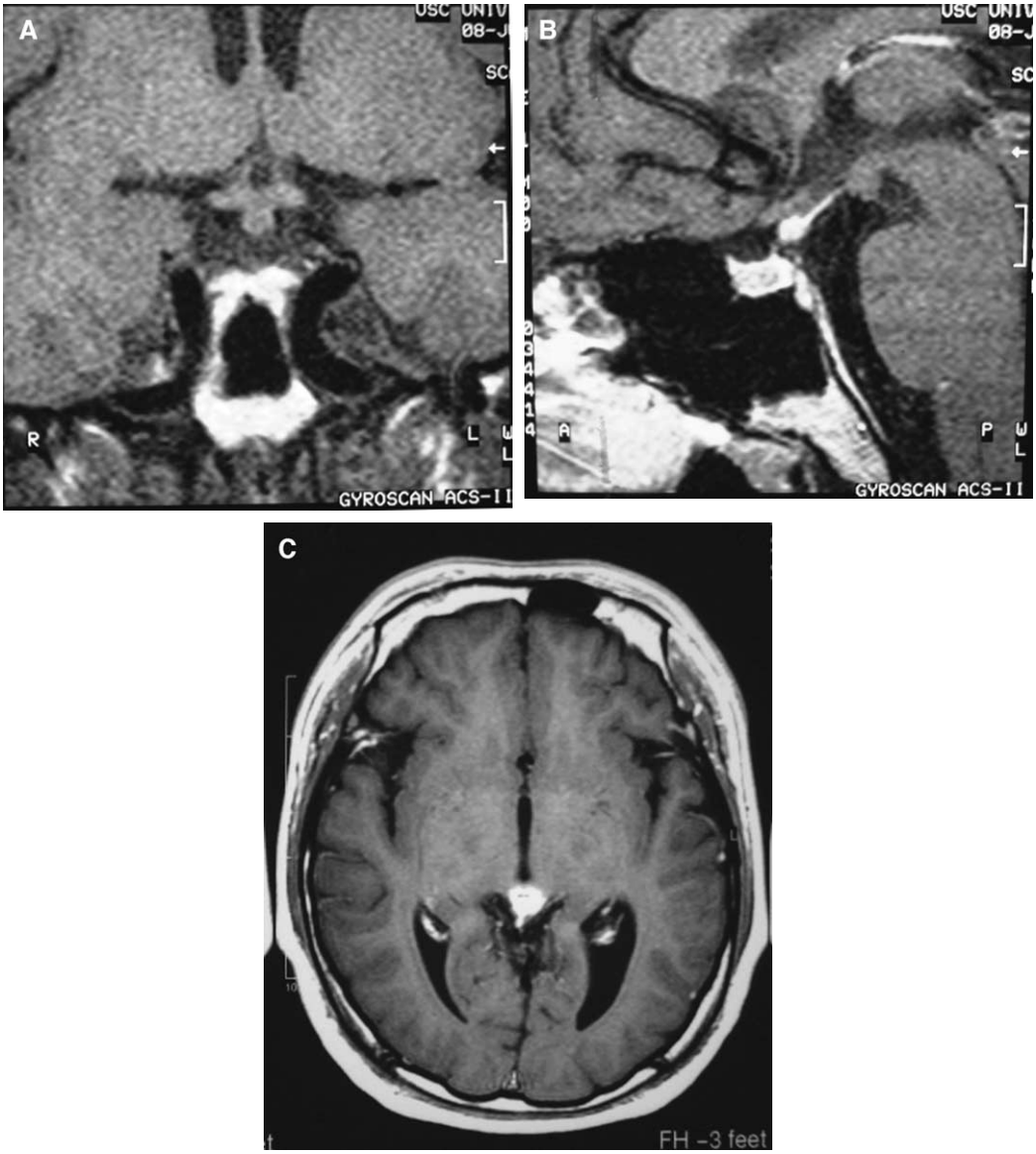

Fig. 16. Suprasellar germinoma with concurrent pineal germinoma. (*A*) Coronal T1-weighted image shows a small suprasellar mass inferior to the chiasm. (*B*) Sagittal postcontrast T1-weighted image demonstrates an enhancing mass along the infundibulum. (*C*) Axial postcontrast T1-weighted image demonstrates an enhancing mass in the pineal region.

Histiocytosis X

Hypothalamic-pituitary Langerhans cell histiocytosis can present with panhypopituitarism or as isolated central diabetes insipidus. Diagnosis is confirmed by histologic examination showing infiltration with CD1a-positive histiocytes [62]. MRI shows an enhancing suprasellar mass (Fig. 20).

Lymphocytic adenohypophysitis

Lymphocytic adenohypophysitis is a rare condition thought to be related to the autoimmune system. Most frequently, it is seen in peripartum women and is associated with evidence of autoimmune endocrinopathy in other organs [63]. It may also be seen in women with no

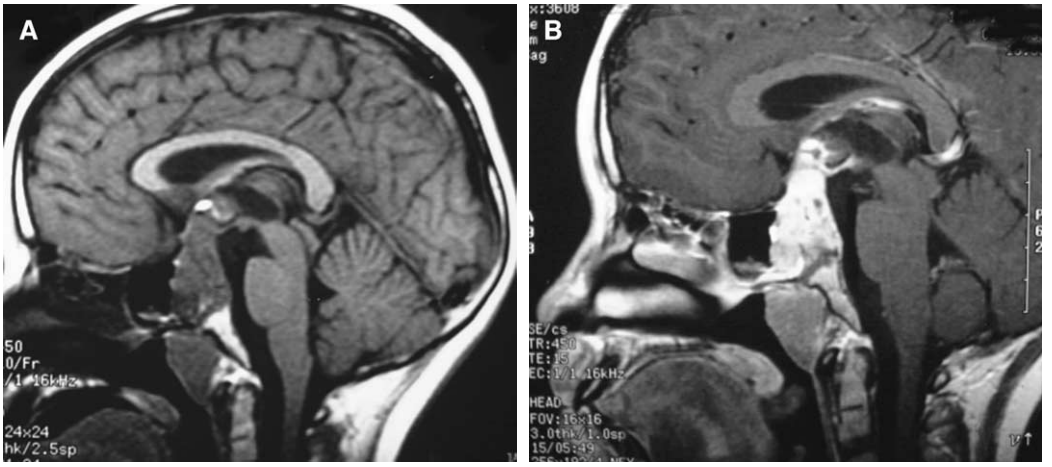

Fig. 17. Mixed germ cell tumor. (*A*) Sagittal T1-weighted image shows a large sellar suprasellar mass of heterogeneous but predominantly isointensity. (*B*) Sagittal postcontrast T1-weighted image demonstrates intense enhancement of the mass lesion with extension superiorly into the hypothalamus and inferiorly into the sphenoid sinus.

recent history of pregnancy, in postmenopausal women, and in men. Histologic study of the involved gland demonstrates a varying degree of infiltration by lymphocytes and other inflammatory cells as well as fibrotic changes. There is a distinct absence of multinucleated giant cells. Similar inflammatory changes may occur within pituitary adenomas as a result of necrosis or hemorrhage within the tumor. Such changes may be indistinguishable from adenohypophysitis even histologically.

Imaging features

MRI

The pituitary gland is usually isointense or slightly hyperintense to gray matter on T1-weighted images and shows intense contrast

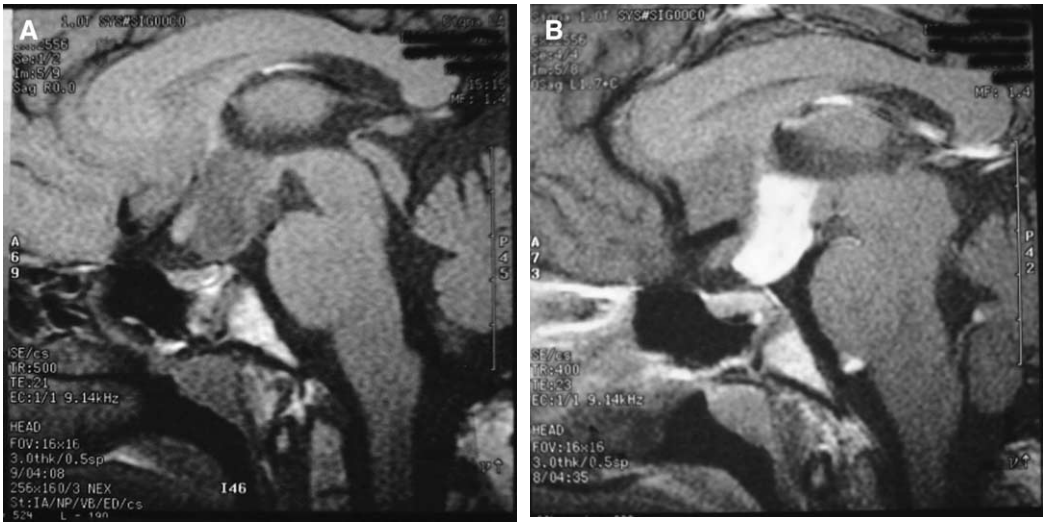

Fig. 18. Metastatic renal cell carcinoma. (*A*) Sagittal T1-weighted image shows a large hypointense suprasellar mass. (*B*) Sagittal postcontrast T1-weighted image shows intense enhancement of the suprasellar mass involving the hypothalamus.

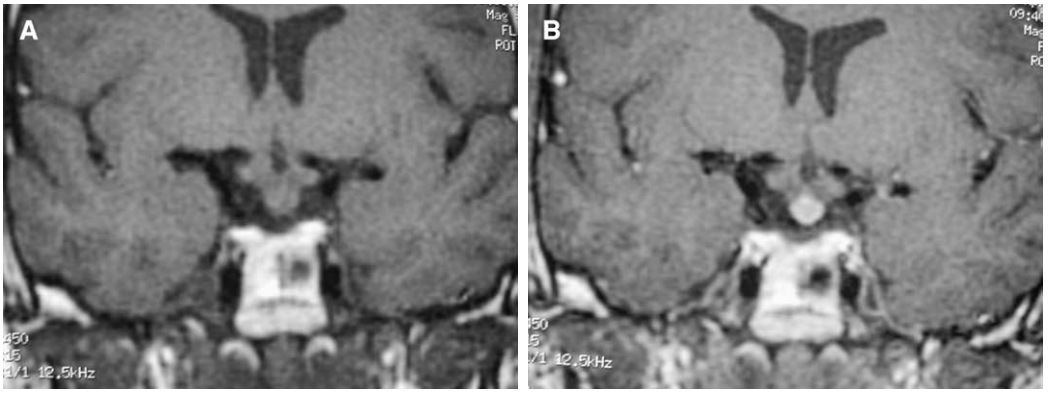

Fig. 19. Sarcoidosis. (*A*) Coronal T1-weighted image demonstrates a suprasellar isointense mass. (*B*) Coronal postcontrast T1-weighted image shows intense enhancement of the mass just inferior to the optic chiasm.

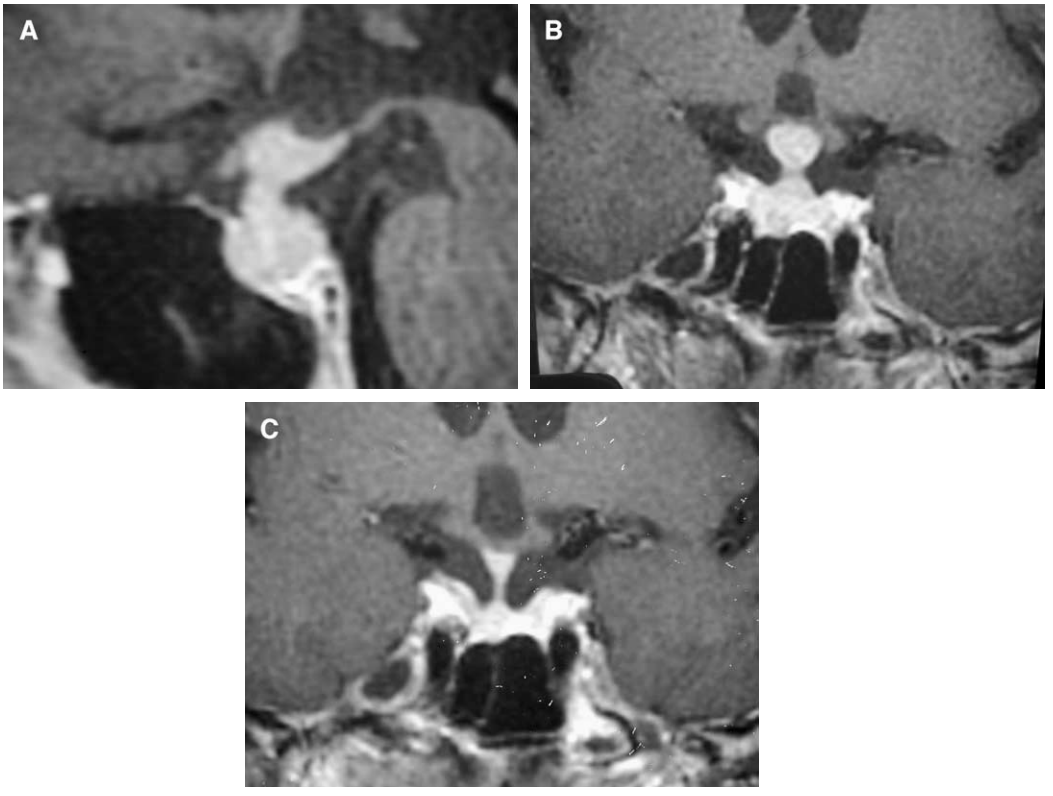

Fig. 20. Histiocytosis. (*A*) Sagittal postcontrast T1-weighted image demonstrates an enhancing mass in the suprasellar region involving the infundibulum. (*B*) Coronal postcontrast T1-weighted image shows an enhancing mass in the suprasellar region along the infundibulum. Compression of the optic chiasm is seen. (*C*) Coronal postcontrast T1-weighted image obtained 3 months later after treatment shows a significant decrease in the size of the mass lesion along the infundibulum.

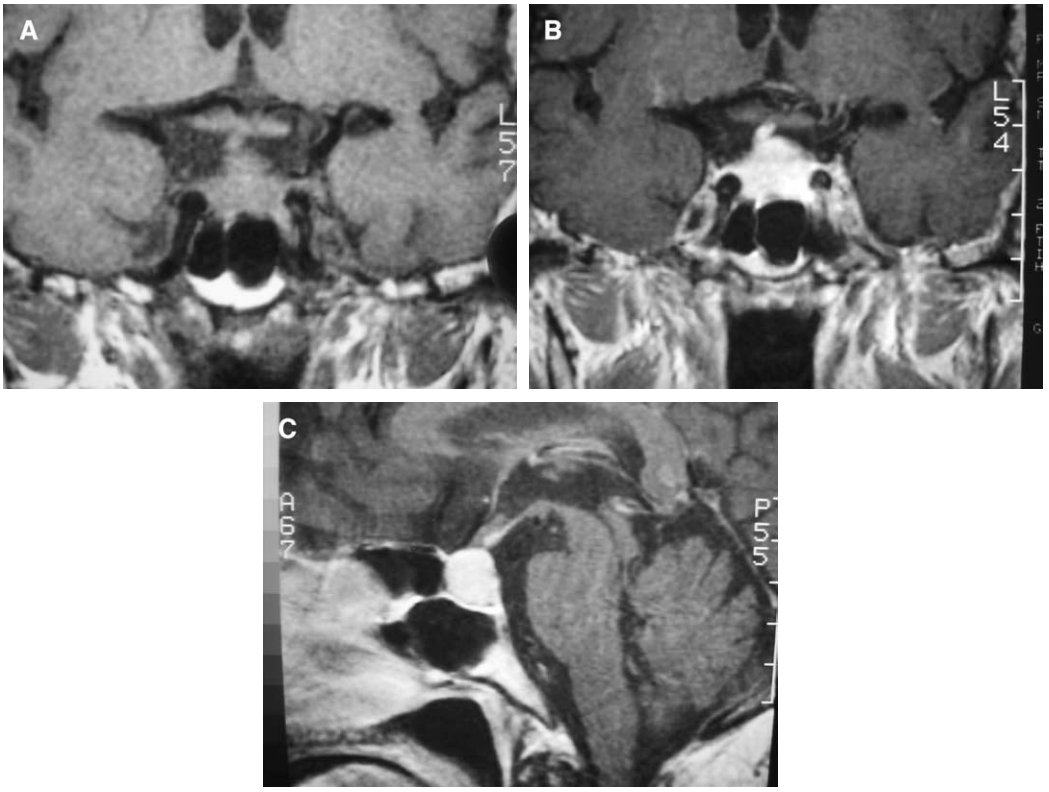

Fig. 21. Lymphocytic adenohypophysitis. (*A*) Coronal T1-weighted image shows a sellar suprasellar mass, mimicking a pituitary adenoma. (*B*) Coronal postcontrast T1-weighted image shows enhancement of enlarged pituitary gland and thickened pituitary stalk. (*C*) Sagittal postcontrast T1-weighted image again demonstrates enhancement of the enlarged pituitary and thickened stalk.

enhancement after intravenous injection of contrast material. A dural tail adjacent to the sellar turcica is frequently seen. Abnormal enhancement of the pituitary stalk extending to the hypothalamus is commonly seen (Fig. 21). Involvement of the cavernous sinus may also be seen [30,64].

Suprasellar aneurysm

There are numerous lesions that may present as suprasellar masses. Of all these lesions, the most important to exclude as a diagnostic possibility is a suprasellar aneurysm. The reason for this importance is the catastrophic consequences of attempted biopsy of a vascular lesion in this region. Aneurysms in this region usually originate from the cerebral vasculature of the circle of Willis or the cavernous carotid artery and project into the suprasellar cistern. The appearance of these lesions may vary widely and is most affected by the amount of calcification and thrombosis present within the aneurysm.

Imaging features

CT

On CT, suprasellar aneurysms are usually hyperdense masses, often with a peripheral rim of calcification. After contrast administration, intense enhancement of a round or oval lesion contiguous with circle of Willis vessels is common. Remodeling of the bony sellar turcica can be seen. It should be noted, however, that if a significant amount of thrombosis is present within the lesion, there may not be contrast filling. CT angiography can be performed to demonstrate the aneurysm as well as its relation to the skull base [65].

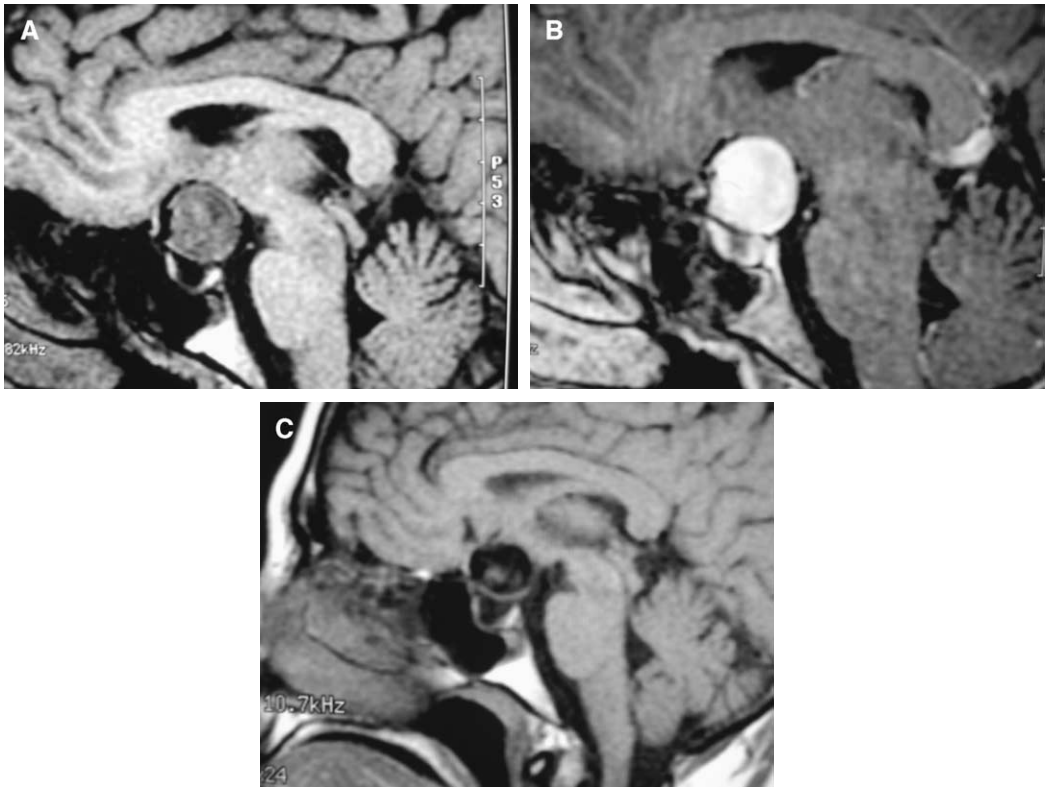

Fig. 22. Large suprasellar aneurysm, mimicking neoplasm. (*A*) Sagittal T1-weighted image using the spoiled grass gradient recalled acquisition in the steady state technique shows a hypointense mass in the suprasellar region. (*B*) Sagittal T1-weighted image shows an intense enhancing mass in the suprasellar region. (*C*) Sagittal T1-weighted image using the spin-echo technique clearly shows the signal void within the aneurysm.

MRI

On MRI, the appearance of these lesions is even more variable and is governed by the amount of flow within these lesions. Again, as previously mentioned, thrombosis is important, because this directly affects flow. In lesions with significant flow, the low signal flow void is visualized in the region of the mass. For lesions with more thrombosis, concentric heterogeneous rings may be present with variable hypersignal and hyposignal on T1-weighted and T2-weighted images. It should also be noted that a spoiled grass gradient recalled acquisition in the steady state (SPGR) usually does not show signal void in an aneurysm; instead, an aneurysm may falsely appear as a solid mass lesion (Fig. 22).

After CT and conventional MRI, if a vascular lesion is still in question, magnetic resonance angiography (MRA) or conventional angiography may be performed for further evaluation. It should be noted that MRA has become quite commonplace and is often performed while the patient is still present in the MR suite [66]. According to our experience, three-dimensional contrast-enhanced MRA is superior to three-dimensional time-of-flight MRA in the evaluation of intracranial aneurysms. If any questions remain or treatment is planned, conventional angiography is still the gold standard.

Neoplasms involving the clivus

Neoplasms in the clival region include chordoma, chondrosarcoma, metastasis, plasmacytoma, lymphoma, and meningioma [67,68]. Clival chordomas are uncommon slow-growing tumors arising from the remnants of the primitive notochord.

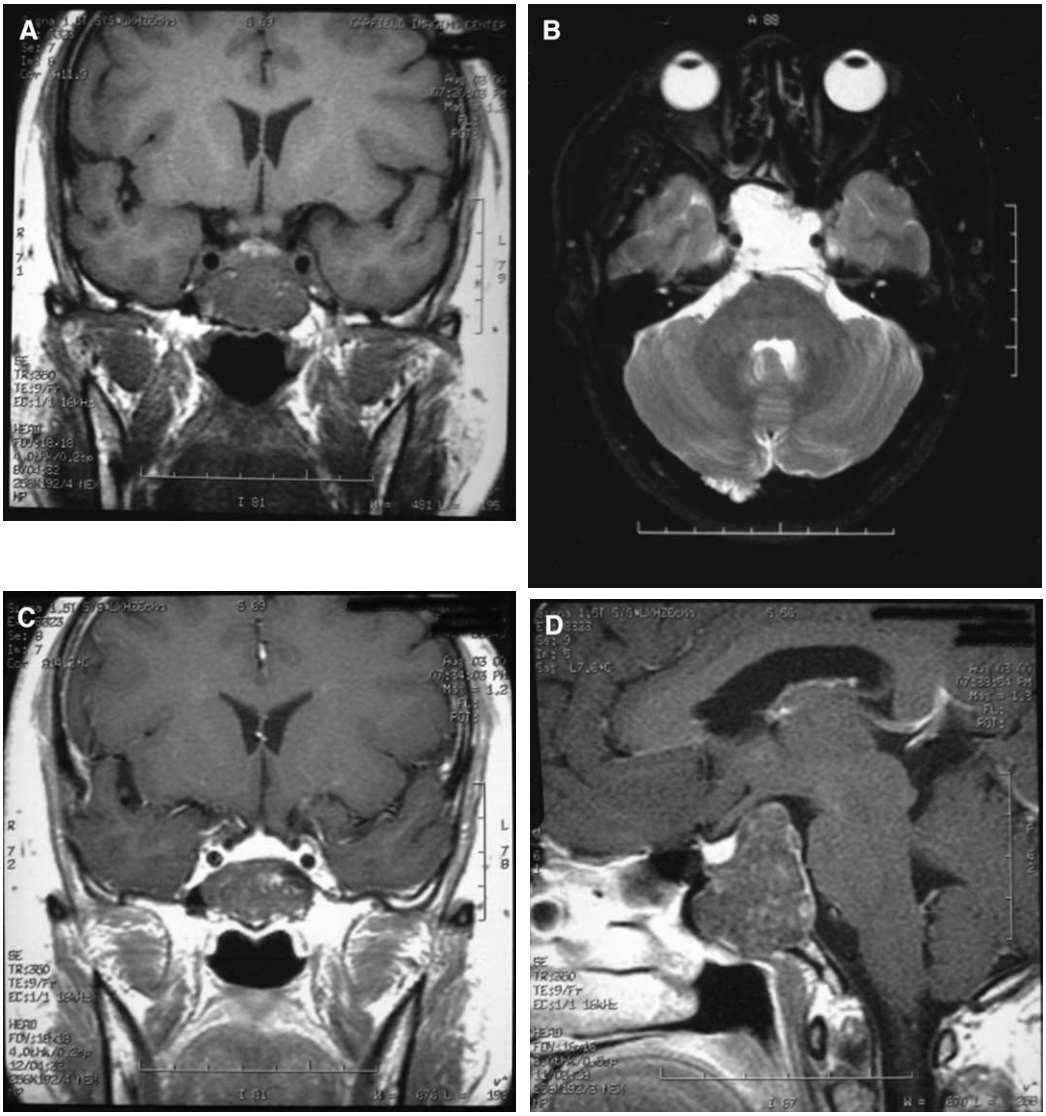

Fig. 23. Chordoma of the clivus. (*A*) Coronal T1-weighted image shows a hypointense mass inferior to the pituitary gland and involving the sphenoid sinus and clivus. (*B*) Axial T2-weighted image shows the mass to be hyperintense. (*C*) Coronal postcontrast T1-weighted image demonstrates slight enhancement of the mass. Note the intense enhancement of the pituitary gland. (*D*) Sagittal postcontrast T1-weighted image shows slight enhancement of the mass with the markedly enhancing pituitary seen at its superior aspect.

Grossly, they are soft gelatinous tumors with bone destruction. On CT, a soft tissue mass with bone destruction is seen. Calcification is seen in the chondroid type of chordoma. On MRI, they are hypointense on T1-weighted images and heterogeneously hyperintense on T2-weighted images. Contrast enhancement is seen on CT or MRI (Fig. 23).

Chondrosarcomas arise from different locations associated with sutures, such as petro-occipital sutures. They are usually more laterally located compared with chordoma. Chondrosarcomas show slow growth compared with chordoma [67]. Imaging findings are similar to chordoma, except for a slightly higher incidence of calcification (Fig. 24).

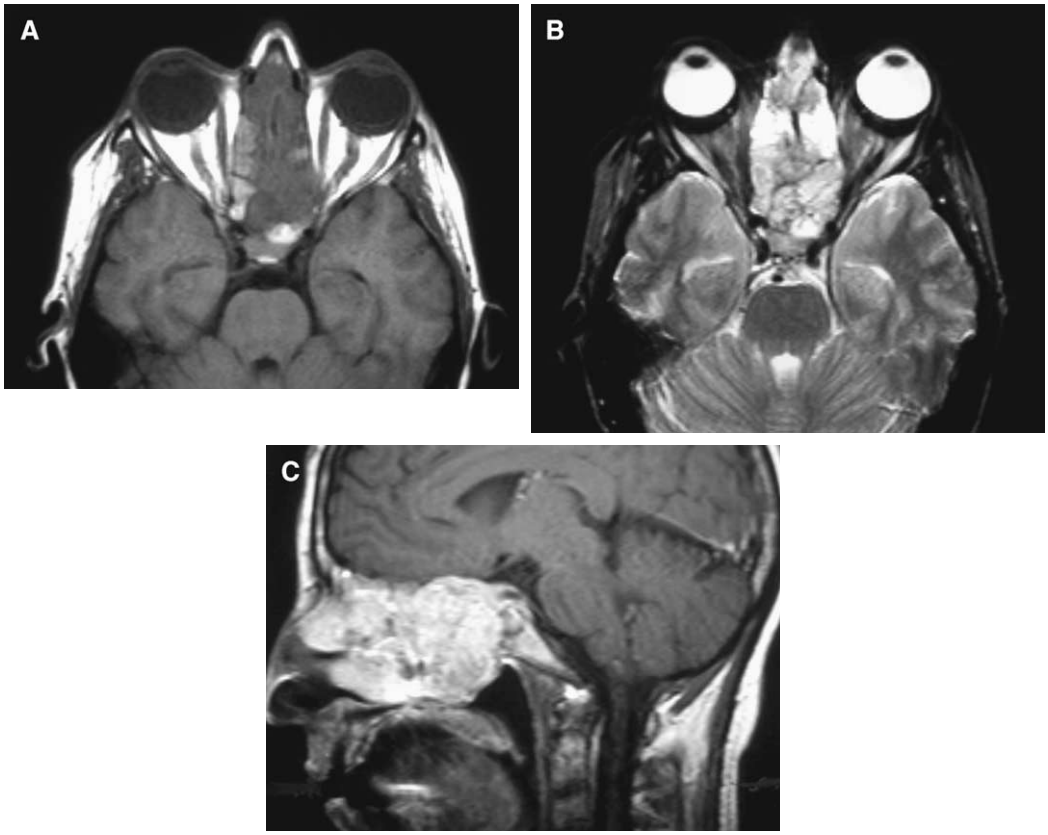

Fig. 24. Chondrosarcoma. (*A*) Axial T1-weighted image shows a mixed signal intensity mass involving the sphenoid and ethmoid sinuses. (*B*) Axial T2-weighted image shows a heterogeneous hyperintense mass. (*C*) Sagittal postcontrast T1-weighted image demonstrates a heterogeneous enhancing mass involving the sphenoid and ethmoid sinuses, with extension into the nasal cavity.

Plasmacytoma and lymphoma can involve the clivus as a part of a systemic disease process. They tend to show lower signal intensity on T2-weighted MRI than chordomas.

Metastasis, lymphomas, and plasmacytomas can all involve the clivus. The signal intensity of metastatic lesions may vary depending on the primary tumor but is generally hypointense on T1-weighted images and hyperintense on T2-weighted images. Lymphoma and plasmacytoma characteristically show hypointensity on both T1-weighted and T2-weighted images.

References

[1] Wiener SN, Rzeszotarski MS, Droege RT, et al. Measurement of pituitary gland height with MR imaging. AJNR Am J Neuroradiol 1985;6: 717–22.

[2] Wolpert SM, Molitch ME, Goldman JA. Size, shape and appearance of the normal female pituitary gland. AJNR Am J Neuroradiol 1984;5: 263–7.

[3] Thorner MO, Vance ML, Horvath E, et al. The anterior pituitary. In: Wilson JD, Foster DW. Williams textbook of endocrinology 1992. Philadelphia, WB Saunders; 221–310.

[4] Ahmadi J, North CM, Segall HD, et al. Cavernous sinus invasion by pituitary adenomas. AJNR Am J Neuroradiol 1985;6:893–8.

[5] Roppolo HMN, Latchaw RE. Normal pituitary gland: microscopic anatomy-CT correlation. AJNR Am J Neuroradiol 1983;4:937–44.

[6] Mark L, Pech P, Daniels D, et al. The pituitary fossa: a correlative anatomic and MR study. Radiology 1984;153:453–7.

[7] Brooks BS, El Gammal T, Allison JD, et al. Frequency and variation of the posterior pituitary bright signal on MR images. AJNR Am J Neuroradiol 1989;10:943–8.

[8] Columbo N, Berry I, Kucharczyk J, et al. Posterior pituitary gland: appearance on MR images in normal and pathologic states. Radiology 1987;165: 481–5.
[9] Tien R, Kucharczyk T, Kucharczyk W. MR imaging of the brain in patients with diabetes insipidus. AJNR Am J Neuroradiol 1991;12:533–42.
[10] Burrow GN, Wortzman G, Rewcastle NB, et al. Microadenomas of the pituitary and abnormal sellar tomograms in an unselected autopsy series. N Engl J Med 1981;304:156–8.
[11] Kernohan JW, Sayre GP. Tumors of the pituitary gland and infundibulum. Atlas of tumor pathology, section X, fascicle 36. Washington, DC: Armed Forces Institute of Pathology, 1956.
[12] Kovacs K, Horvath E. Tumors of the pituitary gland. Atlas of tumor pathology, fascicle 32. Washington, DC: Armed Forces Institute of Pathology.
[13] Wolpert SM. The radiology of pituitary adenomas. Semin Roentgenol 1984;19:53–69.
[14] Scheithauer BW, Kovacs KT, Randall RJ, et al. Effects of estrogen on the human pituitary: a clinicopathologic study. Mayo Clin Proc 1989;64: 1077–84.
[15] Martin JB, Reichlin S. Clinical neuroendocrinology. 2nd edition. Philadelphia, FA Davis, 1987.
[16] Molitch ME, Russell EJ. The pituitary "incidentaloma". Ann Intern Med 1990;112:925–31.
[17] Kucharczyk W, Davis DO, Kelly WM, Sze G, Norman D, Newton TH. Pituitary adenomas: high resolution MR imaging at 1.5 T. Radiology 1986; 161:761–5.
[18] Cottier JP, Destrieux C, Brunereau L, et al. Cavernous sinus invasion by pituitary adenoma: MR imaging. Radiology 2000;215:463–9.
[19] Cattin F, Bonneville F, Andrea I, Barrali E, Bonneville JF. Dural enhancement in pituitary macroadenomas. Neuroradiology 2000;42:505–8.
[20] Nakasu Y, Nakasu S, Ito R, Mitsuya K, Fujimoto O, Saito A. Tentorial enhancement on MR images is a sign of cavernous sinus involvement in patients with sellar tumors. AJNR Am J Neuroradiol 2001;22:1528–33.
[21] Ostrov SG, Quencer RM, Hoffman JC, Davis PC, Hasso AN, David NJ. Hemorrhage within pituitary adenomas: how often associated with pituitary apoplexy syndrome? AJNR Am J Neuroradiol 1989;10:503–10.
[22] Matsuki M, Kaji Y, Matsuo M, Kobashi Y. MR findings of subarachnoid dissemination of a pituitary adenoma. Br J Radiol 2000;73:783–5.
[23] Dina TS, Feaster SH, Laws ER, Davis DO. MR of pituitary gland postsurgery: serial MR studies following transsphenoidal resection. AJNR Am J Neuroradiol 1994;14:763–9.
[24] Steiner E, Knosp E, Herold CJ, et al. Pituitary adenomas: findings of postoperative MR imaging. Radiology 1992;185:521–7.
[25] Kaplan HC, Baker HL, Houser OW, Laws ER, et al. CT of sella turcica after transsphenoidal resection of pituitary adenomas. AJR Am J Roentgenol 1985;145:1131–40.
[26] Teng MM, Huang CI, Chang T. The pituitary mass after transsphenoidal hypophysectomy. AJNR Am J Neuroradiol 1988;9:23–6.
[27] Yoon PH, Kim DI, Jeon P, et al. Pituitary adenomas: early postoperative MR imaging after transsphenoidal resection. AJNR Am J Neuroradiol 2001;22:1097–104.
[28] Young M, Kattner K, Gupta K. Pituitary hyperplasia resulting from primary hypothyroidism mimicking macroadenomas. Br J Neurosurg 1999; 13:138–42.
[29] Russell DS, Rubinstein LJ. Pathology of tumours of the nervous system. Baltimore: Williams & Wilkins, 1989.
[30] Ahmadi J, North C, Segall HD, Sharma C, Hinton D. Lymphocytic adenohypophysitis: contrast enhanced MR imaging in five cases. Radiology 1995;195:30–4.
[31] Zee CS, Go JL, Lefkowitz M, Nelson MD, Apuzzo MLJ. Advanced imaging of intraventricular and paraventricular lesions involving the third ventricle. In: Apuzzo MLJ, editor. Surgery of the third ventricle. 2nd edition. Baltimore: Williams & Wilkins; 1998;317–64.
[32] Kulkarni V, Daniel RT, Pranatartiharan R. Spontaneous intraventricular rupture of craniopharyngioma cyst. Surg Neurol 2000;54:249–53.
[33] Kristopaitis T, Thomas C, Petruzzelli GJ, Lee JM. Malignant craniopharyngioma. Arch Pathol Lab Med 2000;124:1356–60.
[34] Gupta K, Kuhn MJ, Shevlin DW, Wacaser LE. Metastatic craniopharyngioma. AJNR AM J Neuroradiol 1999;20:1059–60.
[35] Ito M, Jamshidi J, Yamanaka K. Does craniopharyngioma metastasize? Case report and review of the literature. Neurosurgery 2001;48:933–5.
[36] Rao KCVG, Fitz CR, Harwood-Nash DC. Craniopharyngiomas in children: neurological evaluation. Rev Interam Radiol 1977;2:149–57.
[37] Ahmadi J, Destian S, Apuzzo M, et al. Cystic fluid in craniopharyngioma: MR imaging and quantitative analysis. Radiology 1992;182:783–5.
[38] Freeman MP, Kessler RM, Allen JH, Price AC. Craniopharyngioma: CT and MR imaging in nine cases. J Comput Assist Tomogr 1987;11:810–4.
[39] Pusey E, Kortman KE, Flannigan BD, et al. MR of craniopharyngiomas: tumor delineating and characterization. AJNR Am J Neuroradiol 1987;8: 439–44.
[40] Nishioka H, Ito H, Miki T, et al. Rathke's cleft cyst with pituitary apoplexy: case report. Neuroradiology 1999;41:832–4.
[41] Gentry LR, Smoker WRK, Turski PA. Suprasellar arachnoid cysts:1. CT recognition. AJNR Am J Neuroradiol 1986;10:7:79–86.

[42] Pierre-Khan A, Capelle L, Brauner R, et al. Presentation and management of suprasellar arachnoid cysts. J Neurosurg 1990;73:355–9.
[43] Igbal J, Kanann I, Al Homsi M. Non-neoplastic cystic lesions of the sellar region: presentation, diagnosis and management of eight cases and review of literature. Acta Neurochir (wien) 1999;141: 389–97.
[44] Steffey DJ, DeFilipp GJ, Spera T, Gabrielsen TO. MR imaging of primary epidermoid tumors. J Comput Assist Tomogr 1988;12:438–40.
[45] Vion-Dury J, Vincentelli F, Jiddane M, et al. MR imaging of epidermoid cysts. Neuroradiology 1987; 29:333–8.
[46] Black KL, Pihol BK. Gliomas past, present and future. Clin Neurosurg 1999;45:160–3.
[47] Davis PC, Hoffman JC Jr, Weidenheim KM. Large hypothalamic and optic chiasm gliomas in infants: difficulties in distinction. AJNR Am J Neuroradiol 1984;5:579–85.
[48] Bliss P, Brader M. The management of gliomas. Br J Hosp Med 1996;55:82–5.
[49] Liu GT. Visual loss in childhood. Surv Ophthalmol 2001;46:33–42.
[50] Matsumoto S, Hayase M, Imamura H, et al. A case of intrasellar meningioma mimicking pituitary adenoma. No Shinkei Geka 2001;29:551–7.
[51] Beems T, Grotenhuis JA, Wesseling P. Meningioma of the pituitary stalk without dural attachment: case report and review of the literature. Neurosurgery 1999;45:1474–7.
[52] Kanda Y, Mase M, Aihara N, et al. Sellar hemangiopericytoma mimicking pituitary adenoma. Surg Neurol 2001;55:113–5.
[53] Morrison DA, Bibby K. Sellar and suprasellar hemangiopericytoma mimicking pituitary adenoma. Arch Ophthalmol 1997;115:1201–3.
[54] el-Kalliny M, van Loveren H, Keller JT, Tew JM Jr. Tumors of the lateral wall of the cavernous sinus. J Neurosurg 1992;77:508–14.
[55] Konovalov AN, Spallone A, Mukhamedjanov DJ, et al. Trigeminal neurinomas. A series of 111 surgical cases from a single institution. Acta Neurochir (Wien) 1996;138:1027–35.
[56] Lo PA, Harper CG, Besser M. Intracavernous schwannoma of the abducens nerve: a review of the clinical features, radiology and pathology of an unusual case. J Clin Neurosci 2001;8:357–60.
[57] Zee CS, Segall HD, Apuzzo MLJ, et al. MR imaging of pineal region neoplasms. J Comput Assist Tomogr 1991;15:56–63.
[58] Saeki N, Uchida D, Tatsuno I, Saito Y, Yamaura A. MRI detection of suprasellar germinoma causing central diabetes insipidus. Endocr J 1999;46:263–7.
[59] Israel ZH, Yacoub M, Gomori JM, et al. Rathke's cleft cyst abscess. Pediatr Neurosurg 2000;33:159–61.
[60] Kroppenstedt SN, Liebig T, Mueller W, et al. Secondary abscess formation in pituitary adenoma after tooth extraction. Case report. J Neurosurg 2001;94:335–8.
[61] Kumar N, Singh S, Kuruvilla A. Pituitary tuberculoma mimicking adenoma: magnetic resonance imaging. Australas Radiol 2001;45:244–6.
[62] Hieronimus S, Hadjali Y, Fredenrich A, et al. Hypothalamic-pituitary Langerhans cell histiocytosis: a diagnostic challenge. Ann Endocrinol 2000; 61:512–6.
[63] Quencer RM. Lymphocytic adenohypophysitis: autoimmune disorder of the pituitary gland. AJNR Am J Neuroradiol 1980;1:343–5.
[64] Alexiadou-Rudolf C, Hildebrandt G, Schroder R, Ernestus RI. Lymphocytic adenohypophysitis mimicking a pituitary macroadenoma. Neurosurg Rev 2000;23:112–6.
[65] Ogawa T, Okudera T, Naguchi K, et al. Cerebral aneurysm: evaluation with three dimensional CT angiography. AJNR Am J Neuroradiol 1996;17: 447–54.
[66] Isoda H, Ramsey RG, Takahara Y, Takabashi M, Kaneko M. MR angiography of aneurysm: modes of various shapes and neck sizes. AJNR Am J Neuroradiol 1997;18:1463–72.
[67] Crockard HA, Steel T, Plowman N, et al. A multidisciplinary team approach to skull base chordomas. J Neurosurg 2001;95:173–83.
[68] Crockard HA, Cheeseman A, Steel T, Revesz T, et al. A multidisciplinary team approach to skull base chondrosarcomas. J Neurosurg 2001;95:184–9.